Microstructured flexible sensors for wearable technologies

by

Shicheng Fan

A thesis submitted in partial fulfillment of the requirements for the degree of

Master of Science

in

Solid State Electronics

Department of Electrical and Computer Engineering
University of Alberta

Abstract

As common electronics in our daily life, various sensors have been frequently used in a diversity of applications like pressure sensors for weight scales and temperature sensors for thermometers. However, most traditional sensors are built on rigid substrates, and this restricts the usage of these sensors for many areas requiring flexible devices, such as invasive healthcare monitoring. Thus, there's a need for developing flexible sensors on flexible and stretchable substrates, especially in emerging applications in internet-of-things. In this thesis, we proposed a new concept, digital microelectromechanical (MEM) sensors based on the insulating-to-conducting transition of devices through mechanical switching, for pressure and strain detection. By adding eco-friendly nanomaterials - cellulose nanocrystals, we greatly improved the response time of our MEM sensors. Furthermore, we optimized our fabrication process to integrate multiple sensors into one device employing polymer microelectromechanical systems. Many practical applications have been demonstrated using our sensors, from hand gesture detection to heart rate monitoring. We also showed that integrated flexible sensors have the potential to control robotic arms and gripping forces in handing physical objects.

Preface

This thesis is submitted for the degree of the Master of Science at University of Alberta. This Master thesis contains results of the research undertaken in the Department of Electrical and Computer Engineering, University of Alberta, from September 2015 to August 2017, under the supervision of Professor Xihua Wang.

Chapter 2 of this thesis is based on a journal publication - Meng L, Fan S, Mahpeykar S M and Wang X. "Digital microelectromechanical sensor with an engineered polydimethylsiloxane (PDMS) bridge structure". Nanoscale, 2017, 9(3): 1257-1262. Meng L and I equally contributed to this work. I was responsible for testing devices, carrying out simulation works and part of sample fabrications. Meng L designed and fabricated devices for testing. Wang X was the corresponding author.

Chapter 3 of this thesis is based on a paper titled "Improved response time of flexible microelectromechanical sensors employing eco-friendly nanomaterials", which has been submitted for publication in Nanoscale. I was the first author of this paper. Li D was responsible for mechanical measurements. Meng L and Zheng W participated in the analysis of the experimental results. Wang X was the corresponding author.

Chapter 4 of this thesis is based on a paper titled "Polymer Microelectromechanical systems (MEMS) for integrated flexible sensors", which has been submitted for publication in Scientific Report. I was the first author of this paper. Meng L was involved in the sample fabrication, and Li D carried out the mechanical test of samples. Wang X was the corresponding author.

Acknowledgement

Table of contents

List of Tables

List of Figures

Chapter 1. Introduction

This thesis concentrates on the development of flexible sensors to detect pressure and strain for wearable technologies. Sensor is a common device in our daily life, for example, we can find pressure sensors in the weight scale, temperature sensors in the thermometer. Most sensors on the market are fabricated on rigid substrates, while flexible sensors are desired for wearable devices in the future. In this chapter, the basic definition of sensor and its figures of merit will be discussed. Moreover, recent research progress of flexible sensors, especially pressure and strain sensors, will be summarized. In the end, the rationale of the thesis will be presented.

1.1 Introduction to sensors

1.1.1 What is a sensor

In the broadest definition, the device that could give an output by responding to different types of input like light, temperature, motion, moisture, pressure or any other changes in quantities can be named as a sensor. Generally, the signal from the output could be either directly visible like color change or shape deformation, or be transformed into readable signals through certain transduction mechanisms.

1.1.2 Figures of merit

In order to evaluate the performance of sensors, a number of figures of merit have been introduced, including sensitivity, limit of detection, response time and repeatability. Here, we will discuss these important parameters that are widely used to characterize sensors.

Sensitivity

Sensitivity is one of the most important parameters of sensors which determines the accuracy of measurement and effectiveness of the device. A sensor's sensitivity could be defined as the change in output (Δy) of the sensor per unit change in the parameter being measured (Δx) as shown in the following equation: [1]

$$S = \lim_{\Delta x \to 0} \left(\frac{\Delta y}{\Delta x}\right) = \frac{dy}{dx}$$

For instance, for strain sensor, the gauge factor is used to define its sensitivity as $GF = \frac{\Delta R}{R}/\varepsilon$, where $\frac{\Delta R}{R}$ is the percentage of resistance change, and the ε represents the change in measured strain. For pressure sensor, the sensitivity is defined as the $S = \Delta X/\Delta P$, here, ΔP represents the applied pressure change and ΔX denotes the quantitative output change which could be resistance, capacitance or voltage for corresponding transduction mechanisms, such as piezoresistive, capacitive, and piezoelectric sensors.

Limitation of detection (LOD)

The limitation of detection, another important performance parameter, is defined as the quantity derived from the smallest signal that can be detected with a distinguishable signal change. For instance, for pressure sensor, the limitation of detection could also be called the threshold pressure, which is referred to the lowest pressure that produces a distinguishable signal change. So, improvement on the LOD of sensors is important for devices to measure subtle signal, like acoustic pressure senor, which required the limitation of detection to be less than 1 Pa.[2]

Response time

Another important parameter for evaluating the performance of sensors is the response time, especially for those used in dynamic real-time sensing conditions. The value of response time

indicates how quickly the responded signal could reach to steady state. For the sensor based on polymers material, the response time can be largely influenced by the viscoelastic property of polymers.[3] In the development of flexible sensors, the parameter of response time becomes more and more important, particularly in instant-response displays and real-time monitoring of health conditions. For now, by using new fabrication structure or material, the response time of many sensing devices have been reduced to less than 10 ms.[4]

Repeatability

Last but not least, the parameter of repeatability plays a key role for the performance of sensors, especially for the commercialized sensors. According to related references, repeatability is the most used parameters for determining the reliability of a measurement system. For repeatability, it refers to the consistency of a single sensing device to produce the same results despite changing working conditions, such as temperature, vibration and time. Taking strain or pressure sensor as example, loading and unloading test is usually conducted to test the repeatability of sensors. In academe, the loading and unloading test cycle for sensors could reach to 10000 times,[5] however, the number of test cycles is not large enough for industrial. To achieve high repeatability, a lot of factors have to be controlled in manufacturing sensors, like design considerations and specialized functionality.

1.1.3 Different Types of Sensors in Electronics

Thanks to the size reduction of sensors, most of us are not aware of that we are living in the world immersed with various sensors. For example, sensors have been frequently applied in our power systems such as electrical and electronics appliances, load control systems, home automation or industrial automation as shown in Fig. 1-1. According to different classifications, sensors can be categorized to various types. Most of time, people categorize sensors from the point of view of

their applications, such as temperature sensors, infrared (IR) sensors, ultrasonic sensors, pressure sensors, proximity sensors, and touch sensors. Therefore, people could easily identify the function of individual sensors from their names. In following paragraphs, I will use the pressure sensor as an example to briefly discuss its working principles and figures of merit.

Figure 1-1. various sensors applied in our power systems such as electrical and electronics appliances, load control systems, home automation or industrial automation.[46]

To date, pressure sensors are indispensable in our daily life like in touch screen devices, biomedical instruments, aviation, marine industry, etc. In general, the pressure is defined as the ratio of a force to the area over which it exposed, so the input signal for pressure sensor could include the force generated by any kind of sources, such as gravity, fluid/gas flow, speed, water

level, and altitude. Regarding different transduction mechanism, the pressure sensor could be classified to various types, such as piezoresistive, capacitive, piezoelectric, optical, etc.

Piezoresistive

Piezoresistive pressure sensors usually transduce the applied pressure into the resistance change of the device. There are a lot of advantages in this type of transduction mechanism like simple device architecture and easy read-out mechanism. The changes in resistance are usually achieved from following mechanisms: 1) the geometry change of the sensing element; 2) the contact resistance (R_c) change between two materials; and 3) the resistivity change of a composite owing to changes in antiparticle separation.

For most common strain sensor, the strain gauge, the working principle is based on the definition of the resistance (R):

$$R = \rho L/A \quad (1)$$

where ρ is the resistivity, L is the length, and A is the area.

The effects of geometry on the piezoresistance are dominant when ρ remains constant and L and A change with applied strain. The sensitivity of this strain gauge is referred as the gauge factor (GF), which is defined as

$$GF = \frac{\Delta R}{R}/\varepsilon \quad (2)$$

ε means strain, ΔR is the change in strain gauge resistance, and R is unstrained resistance of the strain gauge, and the GF values due to the change in geometry is 1-2. [6]

For the second mechanism, the contact resistance change is ruled by the relationship: $R_c \sim F^{-1/2}$ which result from the changed contact area between two materials dues to the applied force (F). For the simple dependence between R_c and F, this kind of piezoresistive sensors have advantages to possess high sensitivity at large operating pressures. To date, such mechanism is popular to be

applied in many piezoresistive strain sensors fabricated by cellulose fibers coated with conductive materials.[7, 8] According to a previous report, ZnO as a conductive material in cellulose fibers has led to large values of GF (GF ≈ 116),[7] which is comparable to those of traditional strain sensors made of silicon materials (GF ≈ 200). [9]

Last but not least, piezoresistive polymer composites have been extensively investigated as strain and force sensing materials in recent years.[10-12] Compared with above two mechanisms, piezoresistive polymers work in different ways. For non-conductive polymers with isolated conductive filling materials, the piezoresistivity of the device comes from the tunneling transport of electrons between conductive fillers.[10] When an external pressure or strain is applied, the distance between adjacent filling materials will change and this will influence the tunneling transport and alter the resistivity of the device. For non-conductive polymers filling with the network of conductive materials like carbon nanotubes (CNTs), the break-up and reforming of percolating conductive pathways is used to explain their conductive mechanisms.[13] In this case, electrons can pass through overlapped nanomaterials within the percolation network. Once the external strain is applied, the percolation pathways will change and influence the electrical resistance of the device.

Capacitive

The capacitance of the parallel plates is defined by the equation:

$$C = \varepsilon_r \varepsilon_0 A / d \ (3)$$

where ε_r is the free space permittivity, ε_0 is the relative permittivity, A is the area of overlap of the two plates, and d is the distance between top and bottom electrodes. Thanks to three variables (ε_r, A, d) in this equation,[14] the capacitance of the sensor could be easily controlled by changing these three parameters. For example, the changes in A could be used to measure the shear force, the

changes in d are applied to measure the normal pressure on the surface and ε_r can be used to measure forces using specially designed materials. Compared with piezoresistive sensors and piezoelectric sensors, capacitive senors have a much simpler working principle which will lead to easy design and data analysis. However, there are also some limitations using capacitive sensors in some healthcare applications. For example, the sensor size should be small for device integration, but the reduced value of capacitance in small capacitive sensors may be difficult to extract from large background noises.

Piezoelectric

Piezoelectricity is another commonly used transduction mechanism for pressure sensors. Piezoelectricity refers to electric field changes inside the sensing material in response to the applied mechanical stress. Thus, the working principle for piezoelectric sensor relies on molecular dipoles.[16] The external applied force causes a charge separation between dipoles in material, which will lead to a redistribution of compensating charges on the electrodes. Because of their high sensitivity and fast response time, piezoelectric sensors are widely used in the detection of dynamic pressures such as vibrations of sound and slip.[17] The most attracting advantage of piezoelectric sensors, compared with peizoresistive sensors and capacitive sensors, is that they do not need the external power source to work. Therefore, piezoelectric sensors are good candidates for developing low-power-consumption or even self-powered sensing devices.[18, 19] Furthermore, although the piezoelectric phenomenon was found in certain types of solid material (i.e. crystal and certain ceramic) at the beginning, more and more flexible thin-film materials have been found with piezoelectric properties, including lead zirconate titanate (PZT), ZnO and Poly(vinylidene difluoride) (PVDF).[20] Owing to their flexibility and ease of processing, these thin-film materials are widely used in many fields, especially for emerging E-skin field where the extraordinary mechanical compliance is highly demanded.[21]

In summary, certain figures of merit for different types of pressure and strain sensors have been listed in Table 1.[2] As mentioned before, different types of sensors have their own advantages and limitations. Like capacitive sensors, even though the value of sensitivity and LOD is not excellent, the response/relaxation time is superior compared with other sensors. While for piezoelectric sensors, the LOD could reach to 0.1 Pa which makes it to be the ideal sensing device for measuring ultra-low signals. Thanks to diversified working principles, piezoresistive sensors could achieve both high sensitivity and ultra-low LOD at the same time, as well as extremely low response/relaxation time like capacitive sensors.

Table 1-1 Summary of pressure sensors and their performance parameters. **2015 IEEE. Reprinted, with permission, from Y. Zang, F. Zhang, C. Di and D. Zhu, Mater. Horiz., 2015, 2, 140-156.[2]**

Types of transduction	Materials	Sensitivity	Limit of Detection (LOD)	Response/relaxation time	Operating voltage
Capacitance	GaN	0.0086 kPa^{-1}			
Capacitance	Alumina ceramic	0.0035 kPa^{-1}	100 kPa		
Capacitance/OFET	PS-b-P2VP	1.76 kPa^{-1}	<17 kPa		50 V
Capacitance/OFET	PDMS/Rubrene	0.55 kPa^{-1}	3 Pa	<10 ms	80 V
Capacitance/OFET	PDMS/Pil2TSi	8.4 kPa^{-1}		<10 ms	100 V
Piezoresistivity	Nanohair	$11.35 \text{ μS kPa}^{-1}$	5 Pa	50 ms	
Piezoresistivity	Tissue/Gold nanowires	1.14 kPa^{-1}	13 Pa	<17 ms	1.5 V
Piezoresistivity	Polypyrrole	133.1 kPa^{-1}	0.8 Pa	50 ms	
Piezoresistivity	PDMS/Nanotube	0.23 kPa^{-1}	50 kPa	≤ 125 ms	
Piezoresistivity	Graphene		100 Pa	9 s	2.5 V
Piezoresistivity	PDMS/SWNTs	1.8 kPa^{-1}	0.6 Pa	<10 ms	
Piezoresistivity/OLED	PSR	$42.7 \text{ Cd m}^{-2} \text{ kPa}^{-1}$	1 kPa	1 ms	10 V
Piezoresistivity	PDMS/PEDOT : PSS/PUD	10.32 kPa^{-1}	23 Pa	200 ms	
Piezoresistivity/OFET	Nanowire/PSR	11.5 kPa^{-1}		<0.1 s	5 V
Piezoelectricity	P(VDF-TrFE)		13.3 Pa		1 V
Piezoelectricity	PVDF	2 V kPa^{-1}	1 kPa		
Piezoelectricity	P(VDF-TrFE)	2.3 kPa^{-1}		0.17 s	
Piezoelectricity	P(VDF-TrFE)	1.1 V kPa^{-1}	0.1 Pa		
Piezoelectricity	ZnO	2.1 μS kPa^{-1}	3.5 kPa	0.15 s	1 V
Piezoelectricity	Polypropylene	0.001 kPa^{-1}	2 Pa		
Piezoelectricity	Titanate/P(VDF-TrFE)	$6.7 \times 10^{-4} \text{ kPa}^{-1}$	200 kPa		15 V
Piezoelectricity/OFET	P(VDF-TrFE)		200 kPa		5 V
Optical waveguide	PDMS	0.2 kPa^{-1}	<1 kPa	300 ms	

1.2 The motivations and advances in the development of flexible sensors

In this section, we will look into the development of flexible sensors.

1.2.1 The strong demand for flexible sensors in emerging applications

For monitoring of human health conditions and body movement, many monitoring methods have been extensively studied, such as electrocardiogram (ECG), electromyography (EMG), and electroencephalography (EEG), cameras for capturing limps and body' s motion.[32] Although these methods are accurate and have been widely used in hospital, they all need sophisticated equipment. Thus, these methods are not suitable for portable usage in long-term monitoring. This need in health and wellness monitoring facilitates the development of flexible sensors, since flexible sensors have advantages like outstanding flexibility, low cost, being portable, ultralight and compatible with large-scale manufacturing.

In this section, we will briefly introduce the most promising application fields for flexible sensor. As an example, various applications of pressure sensors are illustrated in Fig. 1-2.
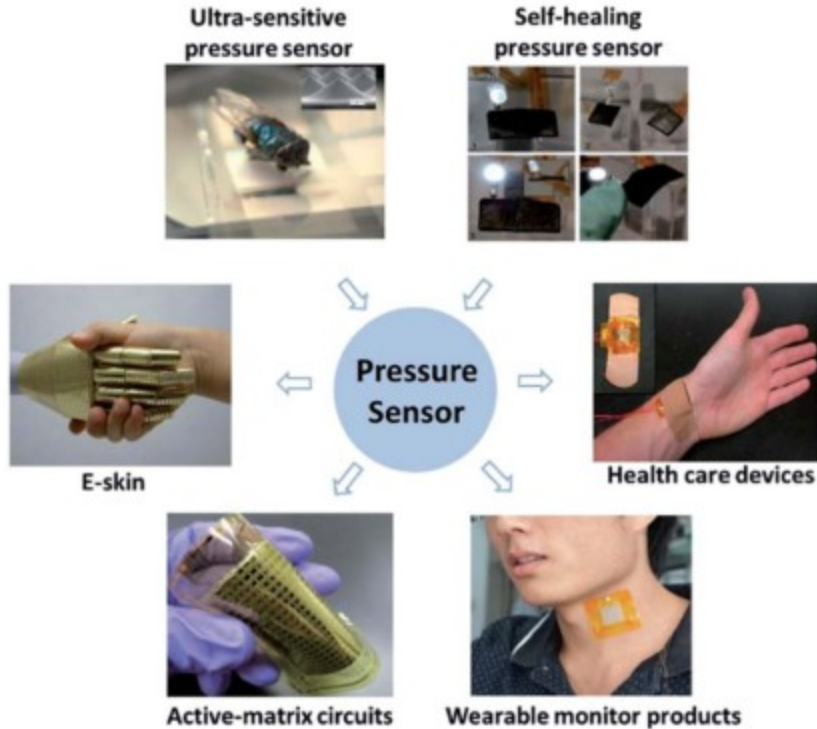
Figure 1-2: various applications for pressure sensor. **2015 IEEE. Reprinted, with permission, from Y. Zang, F. Zhang, C. Di and D. Zhu, Mater. Horiz., 2015, 2, 140-156.[2]**

Mobile biomonitoring

Monitoring human physiological signals like pulse, blood pressure, and heart-beat is always considered to be an effective way for disease diagnosis and health assessment. For this reason, mobile biomonitoring becomes an attractive application in medical diagnostics and health care. As mentioned before, professional medical diagnosis and health assessment are often done in hospitals, while portability of wearable devices is desired for future applications. Recently, flexible and stretchable sensors have attracted a great attention for their extraordinary flexibility and unique capability of detecting subtle pressure changes (less than 1 Pa). These advances may open potential applications for wearable devices in remote health monitoring and assessment.

As showed in Fig. 1-3 a), wearable intelligent bracelets with capabilities to monitor real pulse signal and blood pressure for the collection of fundamental health information have been

produced and are emerging into the market. Progress has also been made in several groups to achieve real-time blood pressure monitoring using flexible sensors. For instance, Bao et al.[33] provides a flexible pressure sensor with a response time of around 10 ms, which is capable to measure the arterial pulse shape with good resolution and could be used to assess a patient's cardiovascular health condition(Fig. 1-3 b, c). In addition, Rogers and coworkers have demonstrated an implantable biomedical device which could measure the electrical activity in heart and brain,[34, 35] and thanks to the mechanical compliance of these flexible substrate, it achieves conformal interaction with these irregular shape organs. (Fig. 1-3 d)
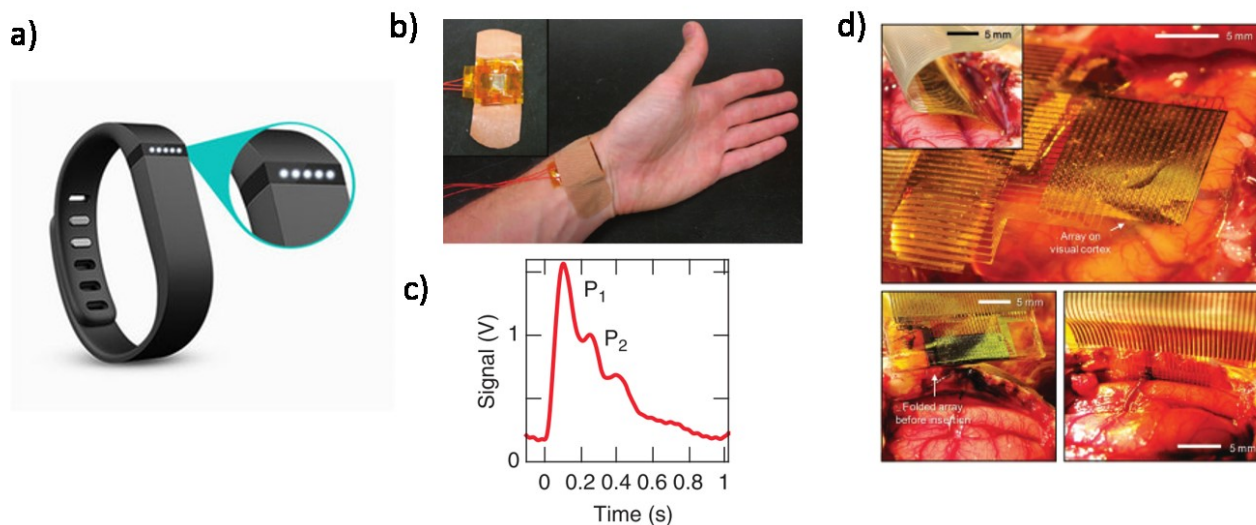
Figure 1-3: a) wearable intelligent bracelets from Fitbit company. b) flexible pressure sensor to measure the arterial pulse. c) pulse signal with good resolution and could be used to assess a patient's cardiovascular health condition. **Reprinted by permission from Macmillan Publishers Ltd: Nature communications[33], copyright (2013).** *d) A flexible, high-density active electrode array was placed on the visual cortex. Inset, the same electrode array was inserted into the interhemispheric fissure.* **Reprinted by permission from Macmillan Publishers Ltd: Nat Neurosci[35], copyright (2011).**

E-skin

Another actively explored application of flexible sensors in the healthcare and biomedical flied is human adaptive artificial electronic skins (AKA e-skins) which could mimic the sensing and transducing abilities like biological skins.[36, 37] In the last few years, Tremendous attention has

been drawn for stretchable e-skins with high sensitivity for their amazing capability to imitate various functions of human skins, such as humidity sensing for skin moisture sensation, thermal heating for body temperature regulation, the ability to interface with the peripheral nervous system and monitor body motion like pressure, strain, shear, vibration, then transducing these data as readable or visible signals. At the same time, these e-skins are highly conformable to soft, curved, and complex surfaces, which enable them to be implemented to any place on our skin. More importantly, the compatibility between e-skin device and human skin is achieved by using biocompatible materials which will avoid the allergy or some other uncomfortable symptoms happen. These properties translate into the potential usage of flexible e-skin in applications such as prosthetic limbs and rehabilitation devices.[37, 38]

Various recent developments in the applications of e-skins have achieved these goals. One of these advances was demonstrated by Kim et al.[37] in their recent studies in which a stretchable smart prosthetic skin based on ultrathin silicon nanoribbons (SiNRs) was developed for sensing signal like pressure, strain, and temperature (Fig. 1-4 a, b). Artificial e-skin laminated on a prosthetic hand could operate a series of complex activities, including handshaking, keyboard tapping, ball grasping, cold/hot drink holding, and wet/dry surface touching (Fig. 1-4 c, d).
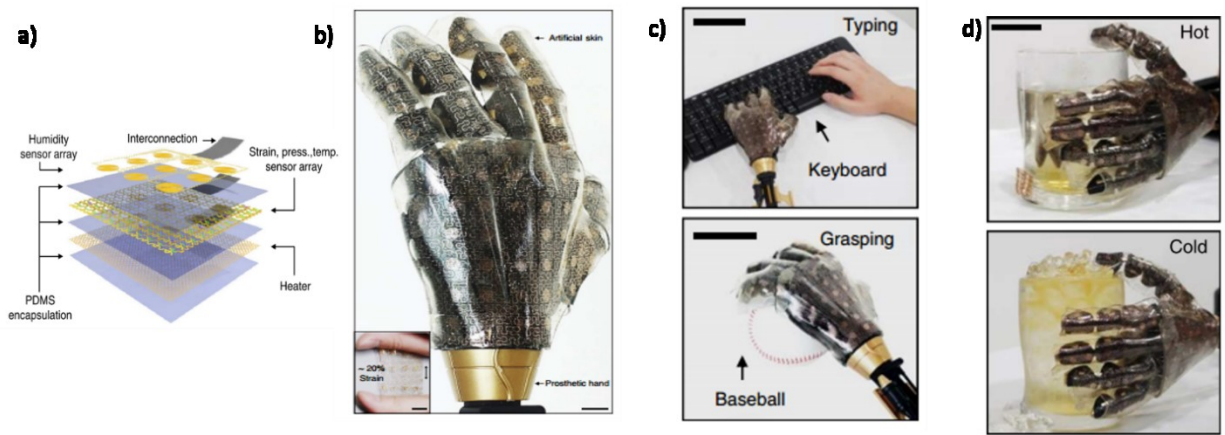
Figure 1-4: Artificial e-skin laminated on a prosthetic hand could operate a series of complex activities. a, b) lamination and integration for smart prosthetic skin. c, d) various applications for smart prosthetic skin. **Reprinted by permission from Macmillan Publishers Ltd: Nature Communications[37], copyright (2014).**

1.2.2 Material development for flexible sensors

The rapid development of flexible sensors in above-mentioned applications benefits from recent advances in the material development. For traditional sensors, common substrate materials are rigid semiconductors or glasses. Flexible sensors require substrate materials to be mechanically flexible and stable under deformation, so common materials like Si or SiO_2[22, 23] are not suitable in this new field. Good candidates for flexible and stretchable substrates are polydimethylsiloxane (PDMS), polyimide (PI), polyethylene terephthalate (PET), polyethylene (PEN) and polyurethane (PU).

Polydimethylsiloxane (PDMS) is by far the most important polymer, which has received considerable attention due to unique properties, such as high transparency, gas permeability, good electric insulation, low surface free energy, excellent weather resistance and low toxicity.[24] The most important characteristic of PDMS is the intrinsic flexibility and mechanical stability under structure deformation like torsion, tensile and compressive strain which enable PDMS to be built for different structure. Another significant property of PDMS is the good compatibility for different composite, with such advantage, by adding conductive particles like carbon nanotube

or graphene, electric insulated PDMS could be converted to conductive material and by adding mechanical enhanced nanoparticle like cellulous nanocrystal (CNC),[25] it could improve the mechanical property and viscoelastic property which have strong impact on the response time to deformation after applied a force.

Polyimide (PI) has excellent stability, insulating property, and mechanical properties.[26] The most important advantage for this material is that it could sustain a large temperature change, from -269°C to 400°C without obvious property changes. More importantly, the chemical immunity property endows it invulnerable to corrosion in commonly used chemical solvents like acetone, alcohol, which helps the PI become the ideal material for subsequent device fabrication process. Like PDMS, PI also has exceptional mechanical property, under intensive mechanical forces or multi-times bending cycle test, no obvious damage or permanent deformation will be left, even for ultrathin film(1mil), which make it to be a suitable choice for flexible device. Last but not least, ultra-lightweight is a promising advantage for PI, especially in e-skin or wearable electronics field, because the ultimate goal for such device is to be inconspicuous after attaching to human body, so the material is needed to be as light as possible.

1.2.3 Novel fabrication techniques

Photolithography is the most standard method to create structures and functional devices on rigid substrates like semiconductor wafers. However, this process is no longer compatible with flexible substrates. Therefore, novel fabrication techniques are proposed to satisfy the need of processing films on the flexible substrate.[27] Although there are plenty of approaches to pattern and deposit materials, various printing techniques are the most promising manufacturing methods. Indeed, printed circuits have already been shown as an attractive alternative for patterning metal wires on flexible substrates, and these printed

wires have excellent electrical conductivity for functional devices.[28] Compared with traditional semiconductor manufacturing techniques, printing shows many advantages. For example, printing is economic and has flexibility in design. Conventional photolithography needs to be performed in strict environment like cleanroom and its equipment is usually expensive and complicated to operate. Moreover, the materials used in photolithography often bring environmental issues.[27] However, for printing techniques, the reduction in material wastages can be achieved by only putting materials in pre-designed areas. Furthermore, some printing techniques like roll-to-roll processing can directly pattern and deposit materials in large areas, in which the size can never be realized in photolithography.

Here two common printing techniques, inkjet printing and screen printing, will be briefly introduced. The basic parameters, as well as advantages and disadvantages, will be discussed.

Inkjet printing is a flexible and versatile technique, and can be set up in relatively low effort. Inkjet printers offering lower throughput of around 100 m²/h and lower resolution (~50 μm) [29] could be a good option for academic research. The advantage of inkjet printing is that it can print on a large variety of substrates including both rigid and flexible substrates. Some of commercially available substrates for inkjet printing are transparent PET films, resin coated papers, glossy photo-papers, polyimide films (Kapton, DuPont). In inkjet printing, the mechanical and electrical properties of printed structures could be easily adjusted by controlling the ink's viscosity and conductivity, as shown in Fig. 1-5. For better adhesion of the ink to the substrate, the substrates may be treated prior to printing. Two of the most widely used pre-treatments are plasma treatment and corona treatment to achieve low roughness, for improving wetting ability of inks.
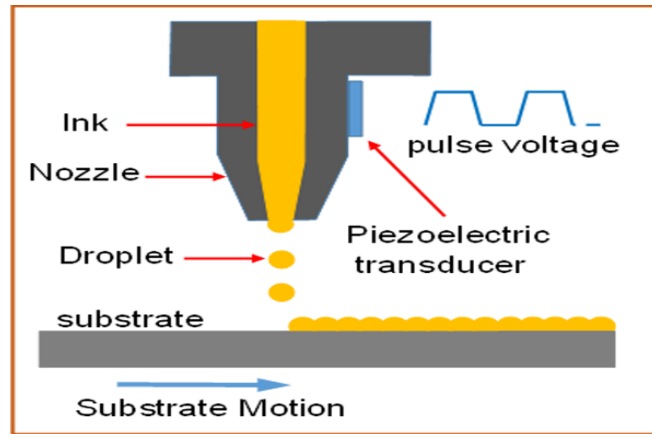
Figure 1-5: Inkjet printing process.[47]

Screen printing is a fast, simple and cost-effective printing technique. It has been used in electronic industry for a long time,[30] and is currently used to print metallic interconnects on print circuit boards (PCB). There are two different work principles for screen printing: flatbed and rotary. For flatbed screen printing, it requires a very simple setup comprising of screen, squeegee, press bed, and substrate, as shown in Fig. 1-6 a). In flatbed, the ink poured on the screen is squeegeed to full across the screen, then the inks will transfer through the stencil openings to the substrate beneath it (Fig. 1-6 a).[31] However, such method has an obvious disadvantage: slow in printing speed. In order to resolve that problem, rotary screen printing is come up as shown in Fig. 1-6 b). Although it provides high speed, some drawbacks are noticed like expensive setup, difficult for cleaning, and the quality of printing affected by too many uncertainties including solution viscosity, substrate material, etc. This method can produce both conducting lines from inorganic materials and insulating layers. Generally, the throughput is about 50 m²/h with a resolution lower than 100 μm. By optimizing the processing condition and materials, the resolution may improve to achieve 30 microns line/space on flexible substrates.[30]
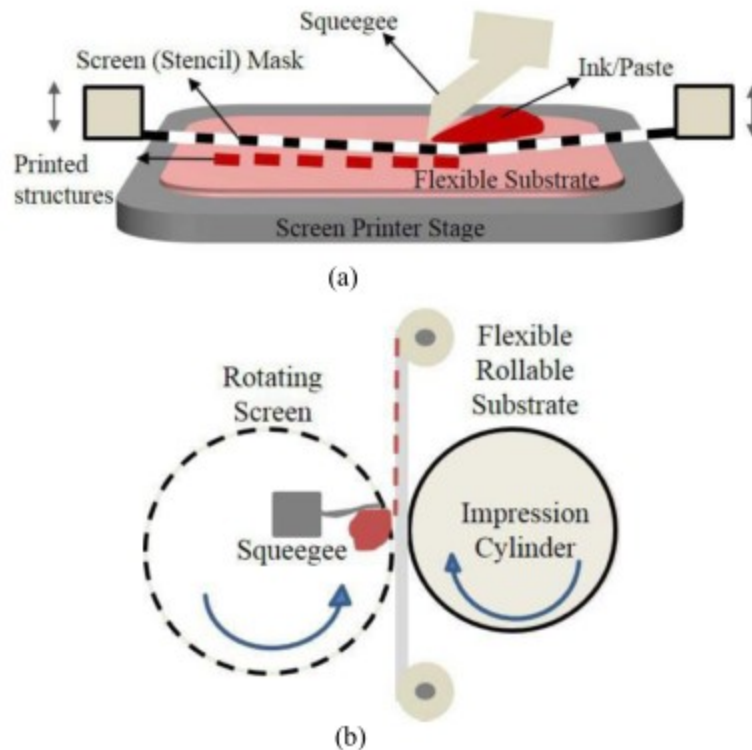
Figure 1-6: (a) The flatbed Screen printing with planar substrates under screen and squeegee for solution dispensing. (b) Rotary screen printer with moving substrate between cylindrical mask and impression cylinder. **2015 IEEE. Reprinted, with permission, from S. Khan, L. Lorenzelli and R. S. Dahiya,** **Technologies for Printing Sensors and Electronics Over Large Flexible Substrates: A** *Review, JSEN, 2015.*[31]

1.2.4 Challenges in design and fabrication

Besides the rapid development of flexible sensors in the past few years, there are many challenges existing in this relatively new field. Here we will discuss these challenges from three aspects including detection range and working area, stimulate type, and integration.

Detection range and working area

For different sensing applications, the detection range and sensing area of flexible sensors have to be designed to fit particular applications. Lack of ubiquitous design is the biggest challenge in the development of flexible sensors. For example, acoustic sensors targeted for applications

associated with hearing aids need to react for the ultra-low-pressures which is usually less than 1 Pa,[39] while for physical sensors to monitor different body actions, the detection values should be much higher. In order to detect the standing and sitting motions, a pressure sensor should work in the range of 10 kPa to 500 kPa, and the same sensor need to sense 1 kPa to 10 kPa for gentle finger touch. While the pressure exerted from weight or hand grip could range from 10 kPa to 100 kPa.[37] Therefore, in order to satisfy these demands for different applications, the pressure sensor should be designed with a typical detection range from less 1 Pa to more than 100 kPa. However, up to now, most flexible sensors only have a narrow detection range.

Another problem in design is the size or working area of sensors for different applications. For example, for prosthetic e-skins, the flexible sensor is required to be large enough to cover all the hand surface, however, for some other biomonitoring devices especially these applications applied inside human body, the size of flexible sensors should be as small as possible to avoid damaging the organs or epidermis skin and be easily and safely conform to soft and complex surfaces like brain or heart. In order to meet the stringent demands for different applications, the flexible sensor should be able to be tailored for different sizes or shapes in particular applications. However, limited by the fabrication techniques and working mechanisms (capacitive, resistive, etc.), changing size would have significant impact on its performance and the fabrication cost.

Stimulus type

Due to the difficulties in device design and fabrication on the flexible substrates, detection mode for most flexible sensors has been limited. For example, one can only monitor one specific tactile stimulus in one direction in strain sensing. To date, none of previous reports is capable of detecting and distinguishing the types and directions of external stimuli except sensor array, and this can pose a big challenge or limitation for future applications. For example, in terms of artificial e-skins for prosthetics,[37] most of sensors are designed to detect the strain signal like finger bending, however, the real stimuli is not a two dimension in-plane strain and can not be

18

probed accurately. For other biomedical applications using wearable devices like blood pressure monitoring, the prosthetic e-skin is not working in this condition. It is desired that flexible sensors should be designed and fabricated to detect multiple external stimuli simultaneously. Moreover, various types of flexible sensors should be integrated together, like blood pressure monitor and skin temperature monitor being put into one device.[40]

Integration

As mentioned in a previous section, the commonly used fabrication method for flexible sensors is the printing technique. Although the screen printing technique is beneficial for the production of large area electronics in rotary manufacturing, the printing quality is affected by various factors such as solution viscosity, printing speed, angle and geometry of the squeegee, snap off between screen and substrate, mesh size and material,[41] leading to the printing results unguaranteed. Moreover, expensive setup and difficult post-clean make the screen printing method not to be an ideal choice in academic research.

In addition to the limitation of fabrication method, the implementation of flexible sensors to the sensing platform is a significant challenge for a lot of applications, especially in the biomedical area. To build up a sensing platform, all components with different sensing capabilities must be effectively integrated onto a single flexible chip. So, the first problem shows up - different sensors need different power sources (AC and/or DC). Moreover, the operating voltages for different sensors could not be the same, even all in DC. Due to limitations of current battery technologies, it is difficult to just use one battery and generate all values of AC and DC power sources through circuits. At the same time, other factors, such as seamless integration with data processors and wireless transmitters, are also crucial for bringing flexible sensors into our daily life. A large amount of financial resources and technical advances are required for system integration.

In the end, despite all the ongoing challenges in the development of flexible sensors, there are encouraging signs to address those highlighted areas. We do believe that the development of flexible sensors will be an exciting and promising area for its promising applications in healthcare and wearable technologies in the future.

1.3 Recent progress in flexible strain and pressure sensors for wearable technologies

While the industry of flexible electronics has grown rapidly in flexible solar cells, thin-film transistors (TFTs), displayers, and printed circuits, new applications of flexible sensors have been demonstrated and pursued in academia. Particularly, functional electronic devices on flexible substrates for sensing pressure and strain are under rapid development in many applications, such as wearable electronics, health-monitoring devices, e-skin products and flexible radio-frequency identification (RFID) tags. Here we summarize key progresses of flexible strain and pressure sensors for wearable technologies.
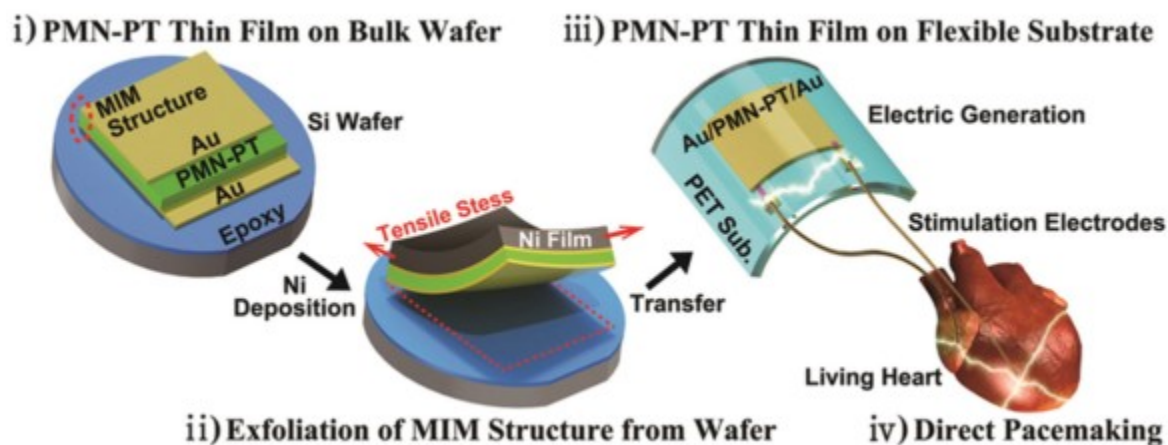
Figure 1-7: The fabrication process for PMN-PT thin-film and the biomedical application for stimulating heart muscle. **Reprinted by permission from Macmillan Publishers Ltd: Advanced Healthcare Materials[42], copyright (2015).**

In order to solve the limitation of battery technology in wearable and healthcare devices, many groups have focused on developing new materials for self-powered sources. For example, Lee et al.[42] developed self-powered energy harvesters for bio-implantable medical devices and achieved high sensitive in physiology signal diagnosis by exploiting the inherent properties of flexible piezoelectric PZT, $BaTiO_3$ films (Fig. 1-7).

To accomplish another challenge of providing fast response for most pressure and strain sensors in wearable systems, especially for those capacitive sensors, many research groups have proposed novel methods to solve this problem. For example, Bao's group at Stanford University has provided a new design of using dielectric pyramidal structures to reduce the effective mechanical modulus of the elastomer by one order of magnitude,[43] (Fig. 1-8 a) which could help pressure sensors to detect the pulse wave inside the radial artery.
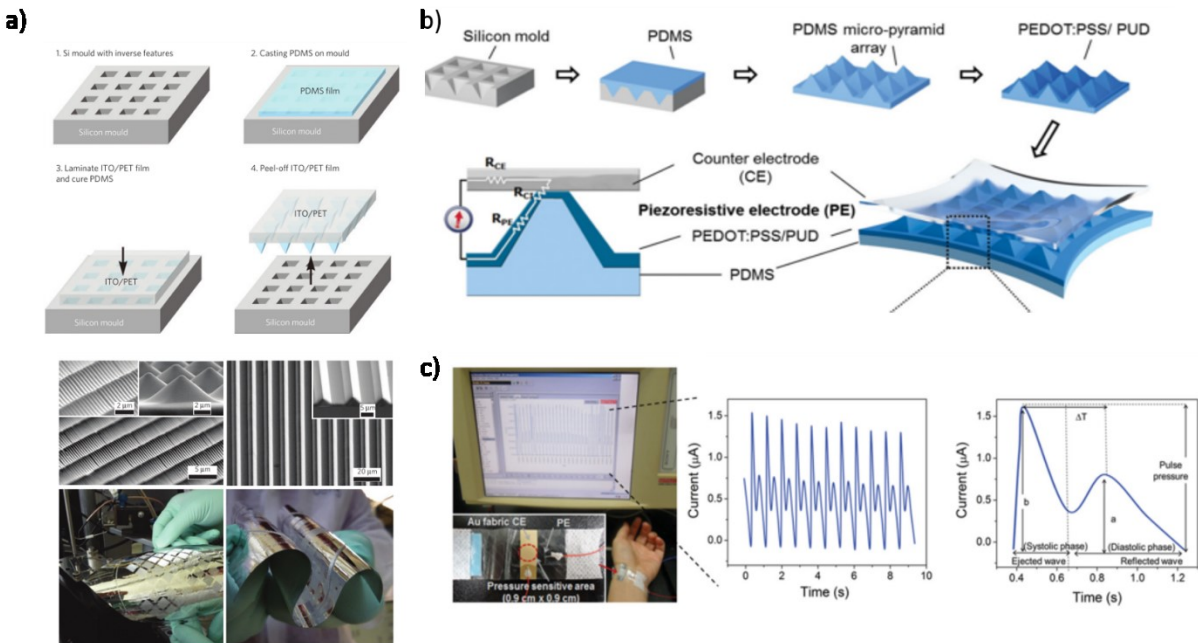
Figure 1-8: Fabrication method for fast response pressure sensor. **Reprinted by permission from Macmillan Publishers Ltd: Nature materials[43], copyright (2010).** *a) Schematic process for the fabrication of microstructured PDMS film. b) fabrication process for sandwich structure of PEDOT: PSS electrodes. c) application for real pulse measurement and characteristic pulse signal analysis.* **Reprinted by permission from Macmillan Publishers Ltd: Advanced Materials[44], copyright (2014).**

The group of Jong-Jin Park has recently demonstrated stretchable and transparent capacitive sensors fabricated by sandwiching a PDMS dielectric between two sets of PEDOT: PSS electrodes.[44] PDMS was used as the dielectric material because of its exceptionally low modulus. According to the definition of Young's modulus, the material with lower modulus will show larger deformation under the same applied force, and this improves sensitivity of the capacitive sensor. Such improvement also enables this pressure sensor to capture real-time arterial pulse waves for health monitoring (Fig. 1-8 b, c).
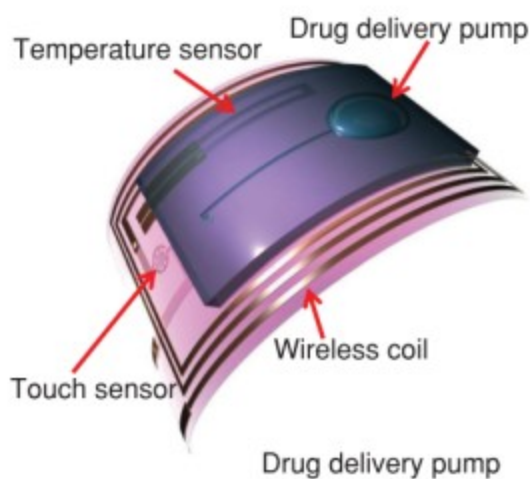
Figure 1-9: Health monitoring device with a temperature sensor, a drug delivery pump, a touch sensor and a wireless coil. **Reprinted by permission from Macmillan Publishers Ltd: Advanced Functional Materials[42], copyright (2014).**

With the demand for multifunctionally wearable devices, flexible pressure and strain sensors are usually integrated into a sensing platform with other types of sensors, like temperature, moisture, and body fluidic sensors. With the longevity of human life and increasing needs for healthcare, insufficiency of physicians and limited healthcare budget become worldwide problems. To address these issues, one potential solution is raised by using flexible pressure and strain sensors to remotely monitor patients for fast response to emergencies. Takei et al. at Osaka Prefecture

University demonstrated an integrated health monitoring device with a temperature sensor, a drug delivery pump, a touch sensor and a wireless coil (Fig. 1-9).[40] Using this device, one can monitor the patient's body temperature and inject the drug when needed.
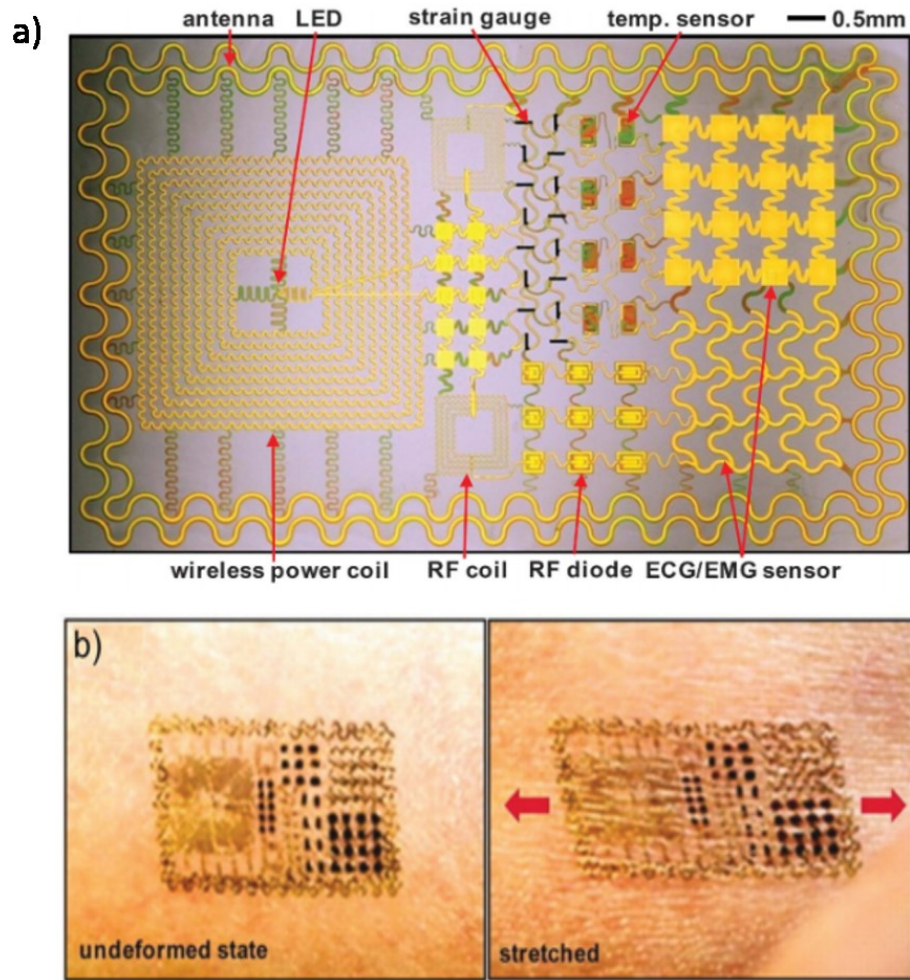
Figure 1-10: Picture of E- skin device. a) epidermal device integrated with various sensors (strain, ECG, temperature). b) strain sensor working on skin. **Reprinted by permission from Macmillan Publishers Ltd: Science [45], copyright (2011).**

John Rogers at the University of Illinois at Urbana-Champaign did a bunch of works on epidermal electronics using transfer printing. As shown in Fig. 1-10, the epidermal device can be tightly attached to the human skin with various sensors (strain, ECG, temperature) integrated into a single device.[45] In the device, one wireless coil is used to remotely provide power for the

LED and the other coil is used for communication purpose. It can output signals produced by sensors to computers or analysis instruments. This work perfectly demonstrates the feasibility of flexible sensors in wearable technologies.

1.4 Outline of the thesis

Flexible stain and pressure sensors are of interest for academia and industry with applications in wearable technologies. Most of such sensors on the market or reported in journal publications are based on the operation mechanism of probing capacitance or resistance changes of materials under applied strain or pressure. In this thesis, we show the design and fabrication of a new class of sensors, digital microelectromechanical (MEM) sensors for wearable technologies. We further improved response time (more than one order of magnitude) of these MEM sensors by employing eco-friendly nanomaterials - cellulose nanocrystals. In the end, we provided a new multi-layer structure fabrication method to integrate multiple digital (MEM) sensors.

In chapter 1, we show the basic definition of sensors, description of various sensors, and the recent development of flexible sensors. Additionally, a brief review of flexible strain and pressure sensor have been given.

In chapter 2, we propose a new concept, the digital MEM sensor, based on the insulating-to-conducting transition of devices through mechanical switching. We fabricated these devices with various sensitivities by engineering the device structures and applied our digital strain sensors to achieve gesture control and heart-beat monitoring.

In chapter 3, we report the dramatically improved response time (more than one order of magnitude) of MEM sensors by employing eco-friendly nanomaterials - cellulose nanocrystals. The incorporation of polydimethysiloxane filled with cellulose nanocrystals has shortened the response time of MEM sensors from sub-seconds to several milliseconds, leading to the detection

of both diastolic and systolic pressures in the radial arterial blood pressure measurement. The demonstrated fast-response flexible sensors enable continuous monitoring of heart rate and complex cardiovascular signals using pressure sensors for future wearable sensing platforms.

In chapter 4, we present a new fabrication method for integration of multiple MEM sensors. Such structure will enable a single sensor with different sensitivities, and by controlling the height for each layer, we could engineer the performance for our sensor. Further demonstrations of our multi-height structure MEM sensor were able to be used for robotic figure gesture monitor and grip force detector.

In chapter 5, we summarize our previous works, and briefly discuss about the future improvement and applications for our digital microelectromechanical (MEM) sensors.

Reference:

1. F. A. M. Davide, C. Di Natale and A. D'Amico, *Sensors and Actuators: B. Chemical,* 1993, **13**, 327-332.

2. Y. Zang, F. Zhang, C. Di and D. Zhu, *Mater. Horiz.,* 2015, **2**, 140-156.

3. S. Gong, D. T. H. Lai, B. Su, K. J. Si, Z. Ma, L. W. Yap, P. Guo and W. Cheng, *Advanced Electronic Materials,* 2015, DOI: 10.1002/aelm.201400063.

4. Y. Lai, B. Ye, C. Lu, C. Chen, M. Jao, W. Su, W. Hung, T. Lin and Y. Chen, *Advanced Functional Materials,* 2016, **26**, 1286-1295.

5. H. Liang, Q. Guan, Z. Zhu, L. Song, H. Yao, X. Lei and S. Yu, *NPG Asia Materials,* 2012, **4**, e19.

6. G. R. Witt, *Thin Solid Films,* 1974, DOI: 10.1016/0040-6090(74)90001-7.

7. X. Xiao, L. Yuan, J. Zhong, T. Ding, Y. Liu, Z. Cai, Y. Rong, H. Han, J. Zhou and Z. L. Wang, *Advanced Materials,* 2011, **23**, 5440-5444.

8. T. Shyr, J. Shie and Y. Jhuang, *Sensors (Basel, Switzerland),* 2011, DOI: 10.3390/s110201693.

9. Hemtej Gullapalli, Venkata S M Vemuru, Ashavani Kumar, Andres Botello-Mendez, Robert Vajtai, Mauricio Terrones, Satish Nagarajaiah and Pulickel M Ajayan, *Small (Weinheim an der Bergstrasse, Germany),* 2010, DOI: 10.1002/smll.201000254.

10. M. Park, H. Kim and J. P. Youngblood, *Nanotechnology,* 2008, DOI: 10.1088/0957-4484/19/05/055705.

11. A Review: Carbon Nanotube-Based Piezoresistive Strain Sensors, (accessed Jul 6, 2017).

12. N. Hu, T. Itoi, T. Akagi, T. Kojima, J. Xue, C. Yan, S. Atobe, H. Fukunaga, W. Yuan, H. Ning and Y. Liu, *Carbon,* 2013, DOI: 10.1016/j.carbon.2012.08.029.

13. Z. Dang, M. Jiang and H. Xu, *Applied Physics Letters,* 2007, DOI: 10.1063/1.2432232.

14. R. Puers, *Sensors and Actuators A: Physical,* 1993, DOI: 10.1016/0924-4247(93)80019-D.

15. W. Hu, X. Niu, R. Zhao and Q. Pei, *Applied Physics Letters,* 2013, DOI: 10.1063/1.4794143.

16. M. G. Broadhurst and G. T. Davis, *Ferroelectrics,* 1984, DOI: 10.1080/00150198408017504.

17. D. P. J. Cotton, P. H. Chappell, A. Cranny, N. M. White and S. P. Beeby, *JSEN,* 2007, DOI: 10.1109/JSEN.2007.894912.

18. R. Yang, S. Xu, C. Xu, Y. Qin, Z. L. Wang and Y. Wei, *Nature Nanotechnology,* 2010, DOI: 10.1038/nnano.2010.46.

19. L. Lin, Y. Xie, S. Wang, W. Wu, S. Niu, X. Wen and Z. L. Wang, *ACS nano,* 2013, .

20. P. K. Panda, *Journal of Materials Science,* 2009, DOI: 10.1007/s10853-009-3643-0.

21. P. Marin-Franch and A. Peláiz-Barranco, *Journal of Applied Physics,* 2005, DOI: 10.1063/1.1847727.

22. H. Gleskova, S. Wagner, W. Soboyejo and Z. Suo, *Journal of Applied Physics,* 2002, DOI: 10.1063/1.1513187.

23. H. Huang and F. Spaepen, *Acta Materialia,* 2000, DOI: 10.1016/S1359-6454(00)00128-2.

24. D. Chen, F. Chen, X. Hu, H. Zhang, X. Yin and Y. Zhou, *Composites Science and Technology,* 2015, DOI: 10.1016/j.compscitech.2015.07.003.

25. A. Pei, J. M. Malho, J. Ruokolainen, Q. Zhou and L. A. Berglund, *Macromolecules,* 2011, **44**, 4422-4427.

26. T. C. Chang, K. H. Wu, C. L. Liao, S. T. Lin and G. P. Wang, *Polymer Degradation and Stability,* 1998, DOI: 10.1016/S0141-3910(98)00011-1.

27. R. F. Pease and S. Y. Chou, *JPROC,* 2008, DOI: 10.1109/JPROC.2007.911853.

28. A. Nathan, A. Ahnood, M. T. Cole, Sungsik Lee, Y. Suzuki, P. Hiralal, F. Bonaccorso, T. Hasan, L. Garcia-Gancedo, A. Dyadyusha, S. Haque, P. Andrew, S. Hofmann, J. Moultrie, Daping Chu, A. J. Flewitt, A. C. Ferrari, M. J. Kelly, J. Robertson, G. A. J. Amaratunga and W. I. Milne, *JPROC,* 2012, DOI: 10.1109/JPROC.2012.2190168.

29. Koji Abe, Koji Suzuki and Daniel Citterio, *Analytical Chemistry,* 2008, DOI: 10.1021/ac800604v.

30. C. Liu and J. Choi, *Journal of Micromechanics and Microengineering,* 2009, DOI: 10.1088/0960-1317/19/8/085019.

31. S. Khan, L. Lorenzelli and R. S. Dahiya, *JSEN,* 2015, DOI: 10.1109/JSEN.2014.2375203.

32. S. Patel, H. Park, P. Bonato, L. Chan and M. Rodgers, *Journal of NeuroEngineering and Rehabilitation,* 2012, **9**, 21.

33. G. Schwartz, B. C. Tee, J. Mei, A. L. Appleton, D. H. Kim, H. Wang and Z. Bao, *Nature communications,* 2013, **4**, 1859.

34. W. Yeo, Y. Kim, J. Lee, A. Ameen, L. Shi, M. Li, S. Wang, R. Ma, S. H. Jin, Z. Kang, Y. Huang and J. A. Rogers, *Advanced materials (Deerfield Beach, Fla.),* 2013, DOI: 10.1002/adma.201204426.

35. J. Viventi, D. Kim, L. Vigeland, E. S. Frechette, J. A. Blanco, Y. Kim, A. E. Avrin, V. R. Tiruvadi, S. Hwang, A. C. Vanleer, D. F. Wulsin, K. Davis, C. E. Gelber, L. Palmer, J. Van der Spiegel, J. Wu, J. Xiao, Y. Huang, D. Contreras, J. A. Rogers and B. Litt, *Nat Neurosci,* 2011, DOI: 10.1038/nn.2973.

36. J. Park, Y. Lee, J. Hong, Y. Lee, M. Ha, Y. Jung, H. Lim, S. Y. Kim and H. Ko, *ACS nano,* 2014, .

37. J. Kim, M. Lee, H. J. Shim, R. Ghaffari, H. R. Cho, D. Son, Y. H. Jung, M. Soh, C. Choi, S. Jung, K. Chu, D. Jeon, S. Lee, J. H. Kim, S. H. Choi, T. Hyeon and D. Kim, *Nature Communications,* 2014, DOI: 10.1038/ncomms6747.

38. T. Yamada, Y. Hayamizu, Y. Yamamoto, Y. Yomogida, A. Izadi-Najafabadi, D. N. Futaba and K. Hata, *Nature Nanotechnology,* 2011, **6**, 296-301.

39. Kenry, J. C. Yeo and C. T. Lim, *Microsystems & Nanoengineering,* 2016, **2**, 16043.

40. W. Honda, S. Harada, T. Arie, S. Akita and K. Takei, *Advanced Functional Materials,* 2014, **24**, 3299-3304.

41. D. Clark, *Graphic Communication,* 2010, .

42. G. T. Hwang, M. Byun, C. K. Jeong and K. J. Lee, *Advanced Healthcare Materials,* 2015, **4**, 646-658.

43. S. C. B. Mannsfeld, B. C. Tee, R. M. Stoltenberg, C. V. H. Chen, S. Barman, B. V. O. Muir, A. N. Sokolov, C. Reese and Z. Bao, *Nature materials,* 2010, **9**, 859-64.

44. C. L. Choong, M. B. Shim, B. S. Lee, S. Jeon, D. S. Ko, T. H. Kang, J. Bae, S. H. Lee, K. E. Byun, J. Im, Y. J. Jeong, C. E. Park, J. J. Park and U. I. Chung, *Advanced Materials,* 2014, **26**, 3451-3458.

45. Dae-Hyeong Kim, Nanshu Lu, Rui Ma, Yun-Soung Kim, Rak-Hwan Kim, Shuodao Wang, Jian Wu, Sang Min Won, Hu Tao, Ahmad Islam, Ki Jun Yu, Tae-il Kim, Raeed Chowdhury, Ming Ying, Lizhi Xu, Ming Li, Hyun-Joong Chung, Hohyun Keum, Martin McCormick, Ping Liu, Yong-Wei Zhang, Fiorenzo G. Omenetto, Yonggang Huang, Todd Coleman and John A. Rogers, *Science,* 2011, DOI: 10.1126/science.1206157.

46. Pinterest; Available from https://www.pinterest.com/pin/169518373454375529/

47. Phys.org - News and Articles on Science and Technology; Available from https://phys.org/news/2015-05-inkjet-kesterite-solar-cells.html

Chapter 2. Digital microelectromechanical sensors on plastic substrates

2.1 Introduction

Strain and pressure sensing are two fundamental sensing functions. Traditional strain sensors use metal foils for good air-stability and reusability. However, a gauge-factor (GF) of only 1-2 can be obtained by metal foil strain gauges, depending on the conductor's geometry.[46] In recent years, various flexible and high-GF strain sensors were demonstrated using new-class of materials, including metal nanoparticles,[47] carbon nanotubes (CNTs),[38] PDMS/metal nanoparticle composites,[48] fabric based materials[49] and polymers.[50] These materials were also employed to develop flexible pressure sensors in recent years.[51-53] For example, Bao et al. applied CNTs on a PDMS substrate to form e-skin with both pressure and strain sensing capabilities.[54] However, the analog-signal output of these sensors requires high standards in device fabrication for mass-production. On the other side, sensors with digital-signal output could provide high tolerance for easy fabrication, and are of interest if these sensors can be engineered to achieve various sensitivities. In 2016, Lai et al. reported an e-skin sensor with digital signal output, which was based on the electrical insulating-to-conducting transition.[55] In the same year, Jiang et al. demonstrated another type of strain sensors with digital signal output using triboelectric effect.[12] Here we presented a new design of flexible microelectromechanical (MEM) sensors, which can switch from insulation to conduction in a tiny amount of time. To our best acknowledgment, this work is the first report of flexible digital sensors with both strain and force sensing abilities. Compared to new-materials based sensors with analog signal output, our digital MEM sensors will set much lower requirements in

fabrication and do not need calibration after long time usage. With engineered sensing structures, digital MEM devices with different sensitivities can be integrated together to achieve the same function as provided by sensors with analog-signal output. Considering the above advantages, digital MEM sensors can be an alternative solution for strain and force sensing in the fields of pressure mapping, sound wave detection and more. In this chapter, we managed to control the sensitivity of the digital MEM sensor by changing the pier height of the PDMS bridge.

2.2 Structure and working principle
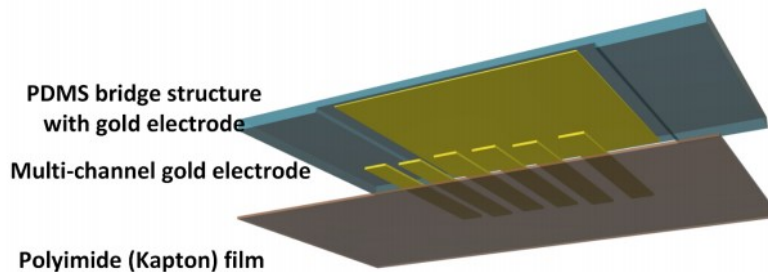
Figure 2-1: Structure of the digital MEM sensors. **Reproduced from Ref. 13 with permission from The Royal Society of Chemistry.**

As illustrated in Fig. 2-1, we chose polyimide film (DuPont, Kapton) as the substrate for bottom electrodes, and used PDMS as the material for the bridge structure. The electrodes on the downside of the bridge structure and on the Kapton substrate are all made of gold with thickness of 60 nm. The distance between the top electrode and bottom electrodes can be controlled by adjusting the height of the piers of the bridge structure. The details of the dimension for this digital MEM sensor is shown in Fig. 2-2.

Cross-sectional view:

Bridge structure | 1 mm

PDMS

Kapton | 125 μm

Gold (60 nm)

Top view:

0.8 cm

1.8 cm | 0.5 cm
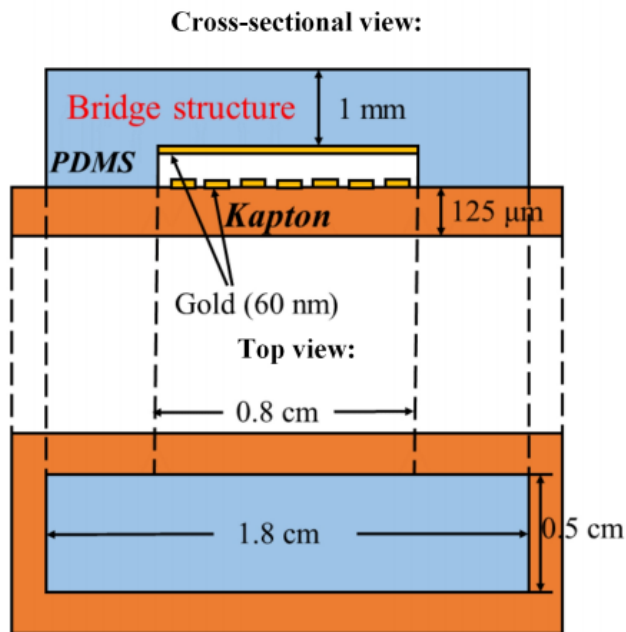
Figure 2-2: Dimension of the digital MEM. **Reproduced from Ref. 13 with permission from The Royal Society of Chemistry.**

Our digital MEM sensors only provide digital signal output. The '0' state means there is no electrical signal between bottom electrodes. When bottom electrodes on the Kapton substrate contact the top electrode on the PDMS bridge, electrical current will be observed under applied voltage. This is referred as the '1' state, in which the conducting channel is formed between bottom electrodes.

relax
bend
press
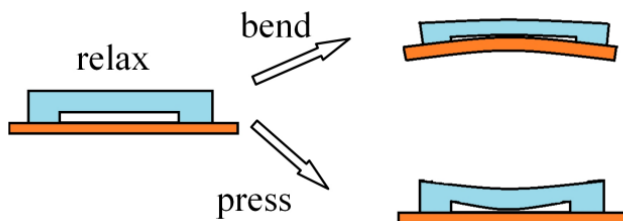
Figure 2-3: Working principle of the digital MEM sensors in two different working modes. **Reproduced from Ref. 13 with permission from The Royal Society of Chemistry.**

As shown in Fig. 2-3, the digital MEM sensor has two working modes. The first mode is the strain sensing mode. In bending test, the PDMS bridge is more likely to be stretched

from tangential direction by the bridge piers while the Kapton substrate is bent in a fixed radius. This will make bottom electrodes contact the top electrode on PDMS to form the conducting channel. The other mode is the pressure sensing mode. Since the Young's modulus of PDMS is much smaller than the Kapton film's, the bridge will touch the Kapton substrate when we apply certain pressures on the PDMS bridge. Thus, the conducting channel is formed between bottom electrodes.

2.3 Experimental

2.3.1 Preparation of PDMS bridge structures
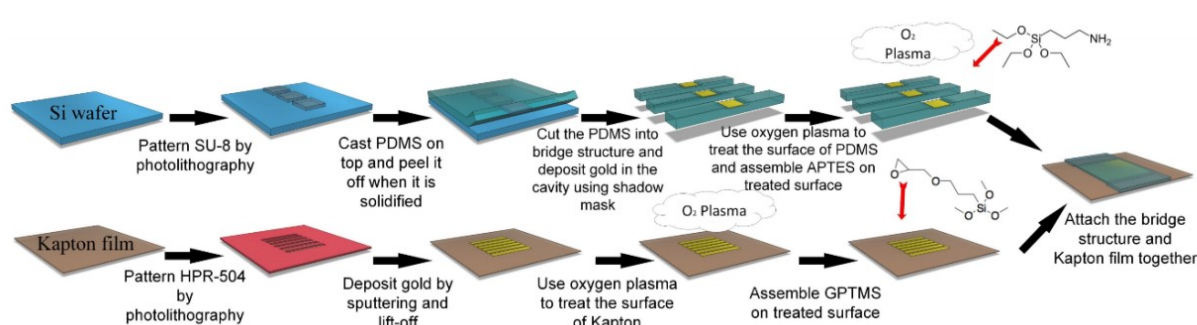
*Figure 2-4: Process flow of the fabrication of digital MEM sensors. **Reproduced from Ref. 13 with permission from The Royal Society of Chemistry.***

As shown in the upper part in Fig. 2-4, the PDMS bridge structures were prepared by soft lithography. At first, SU-8 cuboids of which the thickness can be controlled by the speed of spin-coating were patterned on a piranha-cleaned 4-inch silicon wafer by photolithography.
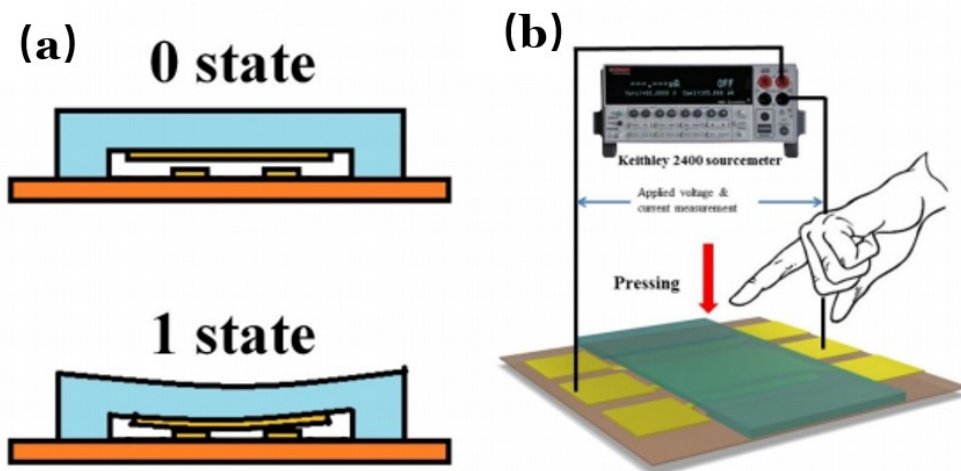
Figure 2-5: a) Schematics of the digital MEM sensor at 0 and 1 states. b) Measurement testing setup illustration. **Reproduced from Ref. 13 with permission from The Royal Society of Chemistry.**

In our experiment, we used three different speed, 1200 rpm, 2000 rpm and 3000 rpm, to produce SU-8 films with the thickness of 124 μm, 90 μm and 58 μm (measured by profilometer), respectively. By controlling the height, we managed to control the sensing ability of our digital MEM sensors. We bent our digital MEM devices using aluminium blocks with different radii. The strain applied to each device was calculated using the method described in our previous work.[13] A Keithley 2400 source meter was employed to apply 0.1 V across two electrodes on the Kapton substrate, and the current passing through these two electrodes was probed by the same instrument. The details of the experimental setup were shown in Fig. 2-5.

Then the wafer was passivated with the vapors of octadecyltrichlorosilane (OTS, SigmaAldrich Inc.) in a vacuum desiccator for over 8 hours. PDMS was prepared from Dow Corning Sylgard 184 kit with a base-to-crosslinker ratio of 10:1. The mixture of base and crosslinker was then degassed, syringed out for 6 ml and poured onto the SU-8 patterned silicon wafer. After being cured at 80◦C for 30 mins, the PDMS will be solidified. Because of the OTS monolayer on the silicon wafer, the PDMS membrane was easy to be peeled off

and cut into bridge structures as we want. At last, 60 nm gold layer with a chromium layer of 10 nm as adhesion layer was sputtered on the bottom of the bridge structure assisted by a PDMS shadow mask.

2.3.2 Preparation of bottom electrodes on polyimide substrate

Gold electrode on polyimide film (DuPont, Kapton) was produced by a lift-off lithography process. HPR 504 photoresist was patterned on Kapton film by photolithography and 60 nm gold layer with 10 nm chromium adhesion layer was sputtered on the Kapton film. A lift-off process by soaking the Kapton film in acetone for 2 hours was then followed.

2.3.3 Bonding of the bridge structure and Kapton film

PDMS bridge structures and Kapton film with gold electrodes were ultrasonically cleaned and activated with oxygen plasma (60 W, 700 mTorr, 60 s). According to the previous report,[15] we immediately immersed the PDMS and Kapton structures into (3-Aminopropyl) triethoxysilane (APTES, Sigma Aldrich Inc.) and (3-Glycidoxypropyl) methyldiethoxysilane (GPTMS, Sigma Aldrich Inc.) water solutions (10%, v/v) for 2 hours. Two water baths were followed to clean them. Then both structures should be well dried and bond together as shown in the last graph in Fig. 2-4. Gentle pressure should be applied on the piers of the bridge structure to make them attached tightly. At last, after 16 h's reaction time, these two structures will be bonded together permanently and irreversibly.

2.4 Results and discussions

Sensors with digital signal output may set high tolerance in device fabrication, but it won't be broadly adopted until the sensor can be engineered to achieve desired sensitivity. In this demonstration, we show various digital MEM sensors with different detection limits by engineering the PDMS bridge structures.
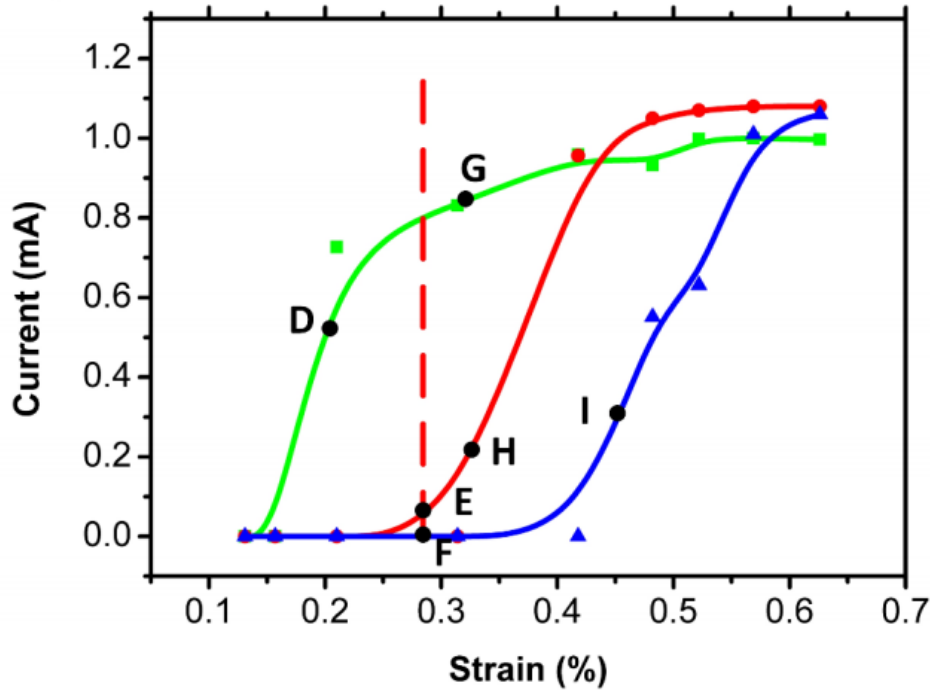
Figure 2-6: Current flowing through the device when different strain applied on Kapton substrate. In this graph, the green, blue and red curves represent sensors with 58 μm, 90 μm, 124 μm. **Reproduced from Ref. 13 with permission from The Royal Society of Chemistry.**

Fig. 2-6 is the electrical current vs. strain curves of three MEM sensors with different pier heights of the PDMS bridge. In the bending test, when we tightened our devices on steel blocks with different radii, these devices were stretched to certain strains. When the radius got smaller, the strain became bigger and the Kapton substrate tended to touch the PDMS bridge. We observed small current when the Kapton substrate gently touched the PDMS bridge, and this current was saturated when two films were firmly touched. Depending on the geometry of the structure, we can design the MEM sensor to achieve different detection limits for strains. As shown in Fig. 2-6, we can clearly see that the threshold strain becomes larger with increasing the pier heights of the bridge.
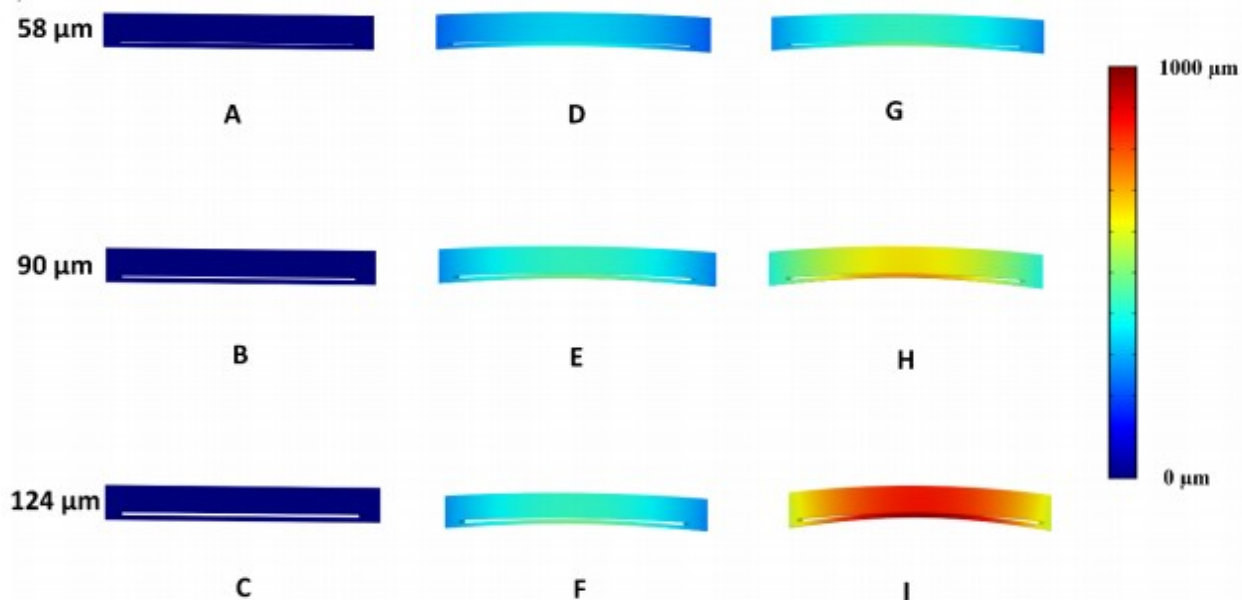
Figure 2-7: Simulated displacement distribution of devices with different pier height in relax and bending conditions. ***Reproduced from Ref. 13 with permission from The Royal Society of Chemistry.***

Simulation results on cross-sections of devices at different bending radii are shown in Fig. 2-7 and they fit well with the experimental results. The simulation was carried out by finite element analysis using COMSOL Multiphysics. In this figure, A, B and C show devices with different pier heights when no strain was applied to the Kapton substrates. G, E and F are the three states that 0.280% strain was applied to the Kapton substrates. At this strain value, the PDMS bridge with 58 μm height was in total contact with the substrate, the PDMS bridge with a pier height of 90 μm showed part contact to the bottom substrate, and the one with 124 μm pier height was not in any contact. From Fig. 2-7, we find that D, H and I state are the three critical transition points for devices changing from the insulation state to the conduction state. The strain values of Kapton substrates are 0.174%, 0.310% and 0.441% for these transition points.
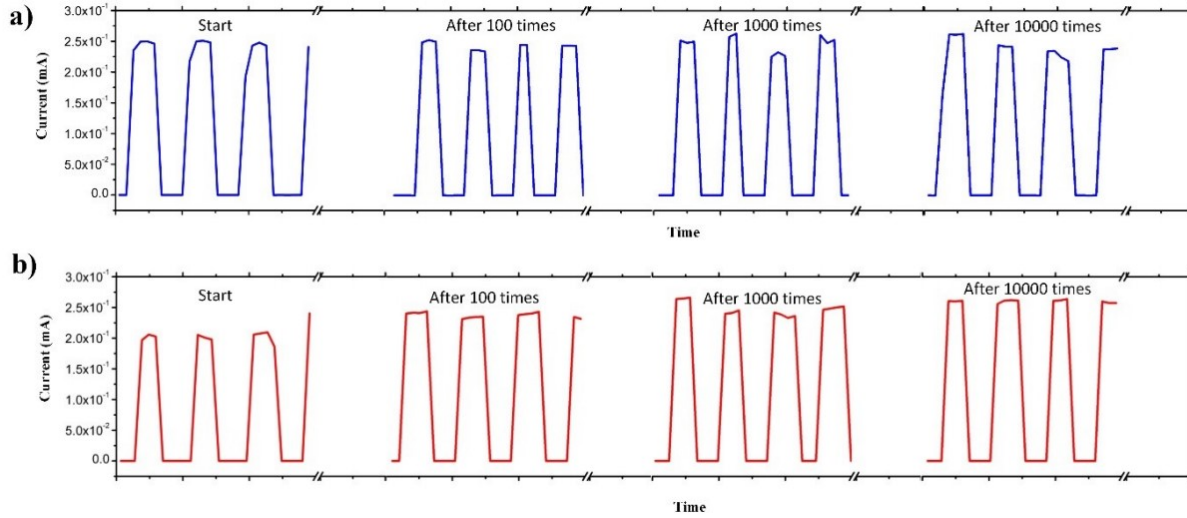
Figure 2-8: a) Durability testing by bending. b) Durability testing by pressing. **Reproduced from Ref. 13 with permission from The Royal Society of Chemistry.**

Our digital MEM sensors also show good reliability in life cycle measurement. The results of the device with 58 μm pier height are shown in Fig. 2-8. We have clearly seen that even after 10,000 times' bending, this device can still work stably in both working modes (forcing sensing and strain sensing). The good stability of our MEM sensors relies on the simple structure design and simple readout mechanism of the device.

For proof of concept, we demonstrated two potential applications of our MEM sensors in each working mode. The readout of our digital MEM sensors only has two states: '1' state for conduction and '0' state for insulation.
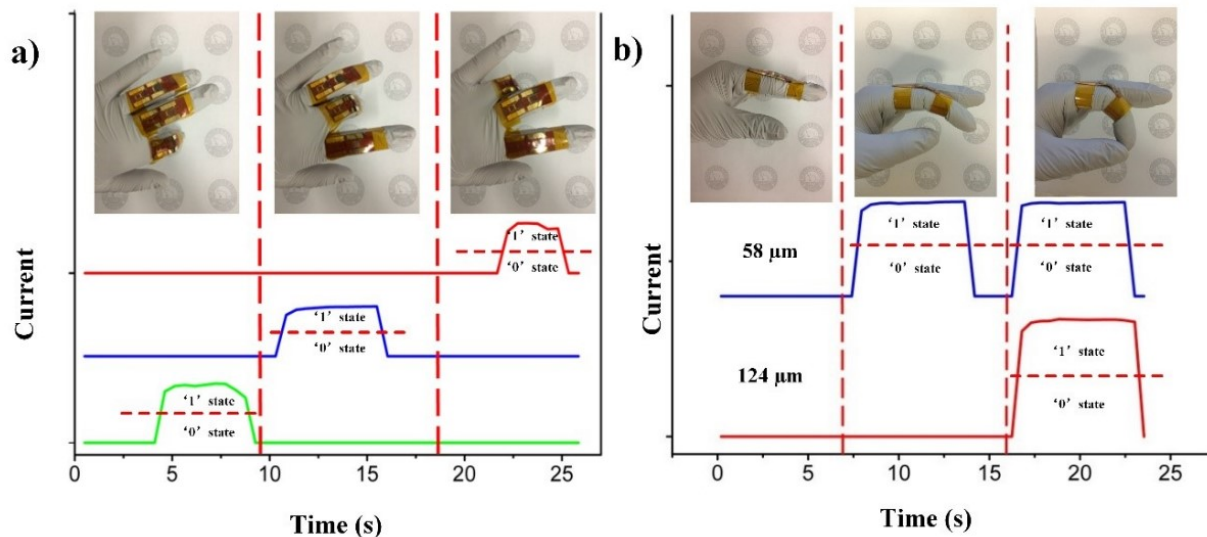
Figure 2-9: a) Response to different fingers bending with digital MEM sensors. b) Digital MEM sensors with different bridge pier heights respond to different bending radii. ***Reproduced from Ref. 13 with permission from The Royal Society of Chemistry.***

As shown in Fig. 2-9 a), we attached devices with 58 μm pier height onto joints of three fingers, index, middle, and ring fingers. When different finger bent, different MEM sensors responded. The output from the device on the index finger is the green curve, the output from the device on middle finger is the blue curve, and the red curve represents the output from the device on the ring finger. This demonstration enables the potential of digital MEM sensors for gesture detection. Furthermore, we integrated two MEM sensors with 58 μm and 124 μm pier heights onto the same finger, as seen from Fig. 2-9 b). According to previous experiments, the smaller value in pier height leads to better detection limit. When the finger slightly bent, only the device with 58 μm pier height showed '1' state in signal output. Further bending made both devices show '1' state in signal output. The extension of this work to more digital MEM sensors integrate on one finger will be able to simulate the function of sensors with analog signal output. We also demonstrated an application of digital MEM sensors for heart rate monitoring using the forcing sensing mode. This was achieved by detecting pressures of wrist pulses on the PDMS bridge.

Figure 2-10: Experimental set-up at human wrist. **Reproduced from Ref. 13 with permission from The Royal Society of Chemistry.**
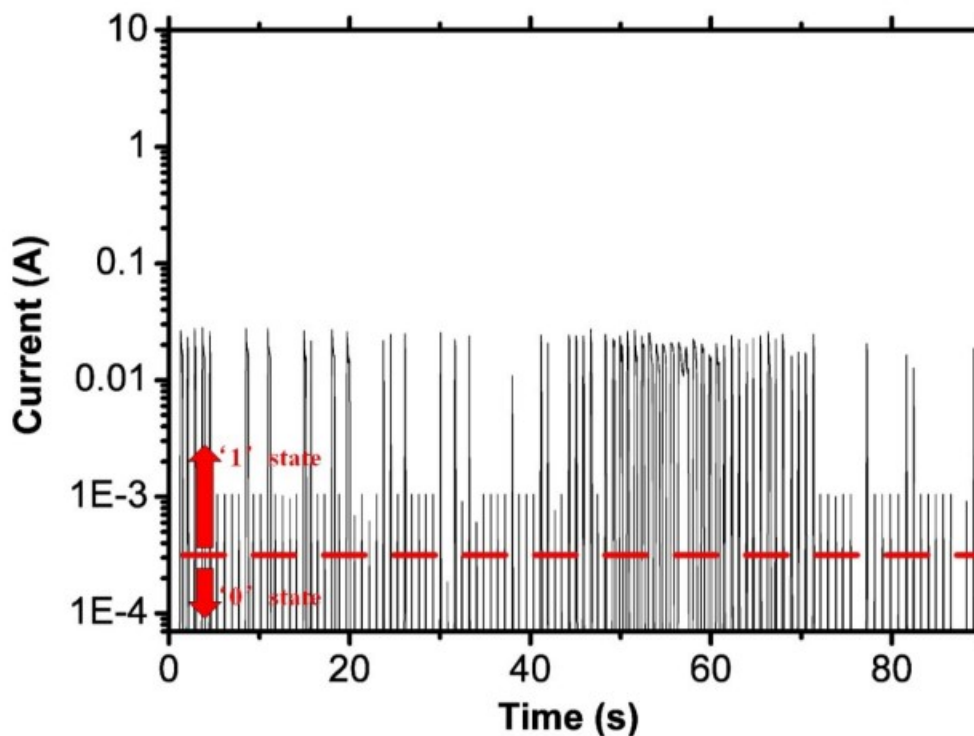
Figure 2-11: Detected heart rate pulses at wrist. **Reproduced from Ref. 13 with permission from The Royal Society of Chemistry.**

Here we used a digital MEM sensor with 58 μm pier height as the wristband as shown in Fig. 2-10 to detect wrist pulses. This demonstration involved a healthy, 24-year-old male. No allergic reactions, redness or damage to the skin were observed in any of our studies. From Fig. 2-11, we observed the visible spikes which should represent the incident waves of blood pressure. Because of the wrist movement or some other unknown factors, some spikes are much lower than normal spikes. However, digital output can still be retrieved from the graph as shown in Fig. 2-11.
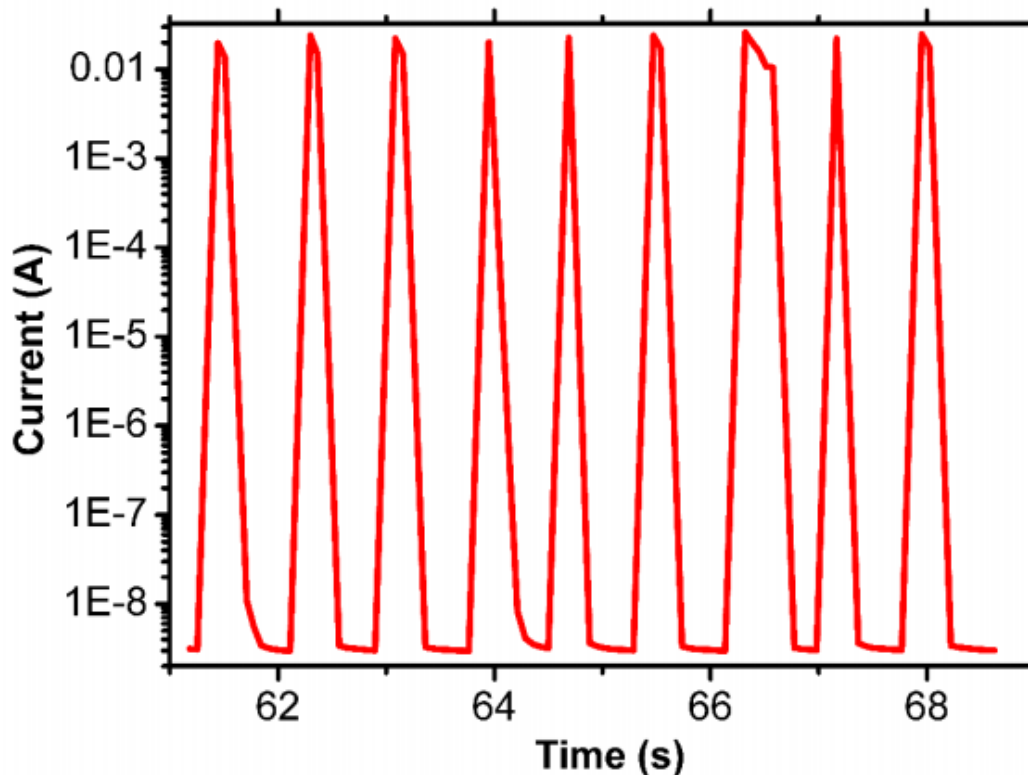
Figure 2-12: Pulse signals in 6 seconds. **Reproduced from Ref. 13 with permission from The Royal Society of Chemistry.**

If we set a low current as the threshold between '1' and '0' states, it is easily to get these two states separated. In a 5 second time zoom-in window (Fig. 2-12), we found that the heart rate of our experimental subject is around 72/min. To verify the reliability of our test results, we also used a commercial sphygmomanometer (Nissei DS-114 computer digital blood pressure pulse monitor) to test the heart rate of the experimental subject at different time of a day and got the result of 71±3/min. This demonstration shows the potential of our devices for small signal detection in the medical field.

Reference

1. W. B. Dobie, P. C. G. Isaac and G. O. Gale, *A-to-Z Guide to Thermodynamics, Heat and Mass Transfer, and Fluids Engineering,* 2006, DOI: 10.1615/AtoZ.e.ELERESSTRGAU.

2. J. L. Tanner, D. Mousadakos, K. Giannakopoulos, E. Skotadis and D. Tsoukalas, *Nanotechnology,* 2012.

3. T. Yamada, Y. Hayamizu, Y. Yamamoto, Y. Yomogida, A. Izadi-Najafabadi, D. N. Futaba and K. Hata, *Nature Nanotechnology,* 2011, **6**, 296-301.

4. Y. Joo, J. Byun, N. Seong, J. Ha, H. Kim, S. Kim, T. Kim, H. Im, D. Kim and Y. Hong, *nanoscale*, Royal Society of Chemistry, 2014.

5. N. Luo, W. Dai, C. Li, Z. Zhou, L. Lu, C. C. Y. Poon, S. C. Chen, Y. Zhang and N. Zhao, *Advanced Functional Materials,* 2016, **26**, 1178-1187.

6. Taeksoo Ji, Soyoun Jung and V. K. Varadan, *LED,* 2007, DOI: 10.1109/LED.2007.909977.

7. Y. Lai, B. Ye, C. Lu, C. Chen, M. Jao, W. Su, W. Hung, T. Lin and Y. Chen, 2016, 1-10.

8. Takao Someya, Tsuyoshi Sekitani, Shingo Iba, Yusaku Kato, Hiroshi Kawaguchi, Takayasu Sakurai and George M. Whitesides, *Proceedings of the National Academy of Sciences of the United States of America,* 2004, DOI: 10.1073/pnas.0401918101.

9. Y. Jiang, S. Li, Z. M. Wang and J. Wu, *Nanoscale sensors*, Springer, Cham [u.a.], 2013.

10. D. J. Lipomi, M. Vosgueritchian, B. C. -. Tee, S. L. Hellstrom, J. A. Lee, C. H. Fox and Z. Bao, *Nat Nano,* 2011, DOI: 10.1038/nnano.2011.184.

11. Y. Lai, B. Ye, C. Lu, C. Chen, M. Jao, W. Su, W. Hung, T. Lin and Y. Chen, *Advanced Functional Materials,* 2016, DOI: 10.1002/adfm.201503606.

12. X. Jiang, Y. Sun, Z. Fan and T. Zhang, *ACS nano,* 2016.

13. L. Meng, S. Fan, S. Milad Mahpeykar and X. Wang, *nanoscale*, Royal Society of Chemistry, 2013.

14. L. Meng, S. M. Mahpeykar, Q. Xiong, B. Ahvazi and X. Wang, RSC Adv., 2016, 6, 85427–85433.

15. Linzhi Tang and Nae Yoon Lee. A facile route for irreversible bonding of plastic-pdms hybrid microdevices at room temperature. *Lab on a Chip*, 10(10):1274–1280, 2010.

Chapter 3. Improved response time of flexible microelectromechanical sensors employing eco-friendly nanomaterials

3.1 Introduction

Flexible sensors integrate functional electronics and other components onto flexible or stretchable substrates to sense physical signals, such as strain, pressure, motion, temperature, etc. Such flexible sensor-integrated systems have huge potential for wearable electronics,[1] health monitoring devices,[2] e-skin products,[3] robotics,[4–6] and prosthetics.[7] Most of previously reported pressure sensors focus on the development of new classes of materials, including but not limited to carbon nanotubes,[3,8,9] graphene and 2D semiconductors,[10] metal nanowires and nanoparticles,[11,12] polymers[13] and their mixtures, and probe capacitance and/or resistance changes of these materials under pressure. Recently, the authors reported microelectromechanical (MEM) sensors like mechanical switches for hand gesture detection and heart rate monitoring.[14] These MEM devices show that micro-/nanostructured device architectures can also bring new functions to flexible sensors.

Polydimethylsiloxane (PDMS), the bridge material in the previous report[15], is a common polymer for adhesives, fabric finishing agents, micro-/nanofluidic, etc., and is especially used in flexible and stretchable electronics for its excellent properties of high transparency, gas permeability, good electric insulation, low surface free energy, excellent weather resistance and low toxicity.[16] However, PDMS also has disadvantages, such as poor mechanical properties (an inherent weak interaction between PDMS chains) and

viscoelastic properties.[16] As a result of these problems, many reports[17–19] show that flexible sensors fabricated of PDMS suffer from a large time-delay in deformation under applied stress. For example, Bao et al.[20] provided a solution by using pyramid structured PDMS electrodes to improve the response time of their flexible sensors.

Here we provide an effective solution for improving the response time of PDMS deformation under applied stress using eco-friendly nanomaterials – cellulose nanocrystals (CNC) – as fillers inside PDMS. As a material extracted from wood and other plants, CNC has been approved for unrestricted use in Canada and is the first nanomaterial included on Canada's Domestic Substances List. In this article, we show that the Young's modulus, storage modulus, and loss modulus of PDMS are dramatically increased by the addition of CNCs into the PDMS film. Thus, the response time of MEM sensors has been improved from sub-seconds to several milliseconds. MEM sensors having the same PDMS structure but with different CNC concentrations also show noticeable shifts in the detection limit, which can add another degree of freedom to control the detection limit of MEM sensors. Finally, we applied MEM sensors in radial artery blood pressure measurement, and successfully detected both diastolic and systolic pressures. The analysis shows that our MEM sensors have the potential to be used in continuous monitoring of heart rate and complex cardiovascular signals

3.2 Experimental

3.2.1 Material

Cellulose nanocrystals(CNCs) were provided by the Alberta Innovates Technology Futures (AITF, Edmonton, AB, Canada). Typical cellulose nanocrystals isolated from cotton or wood have lengths of around 100-300 nm and widths of less than 10 nm.[21] Therefore, the aspect ratio (L/D) of our CNC samples is 10:1-30:1. Sylgard 184 silicone elastomer kit was

purchased from Dow Corning, and which includes the cross-linker and polydimethylsiloxane (PDMS) elastomer.

3.2.2 Prepare CNC/PDMS nanocomposite film

CNC/PDMS nanocomposite films with different weight ratio of CNC (0%; 5%; 10%; 20%) are shown in Fig. 3-1, and were prepared by the following steps. First, the desired concentration of CNC powder was added into PDMS elastomer, which is gel-like as the precursor. The amount of each component was selected based on the concentration desired to form 2.0 g of mixture. Then cross-linker curing agent with the ratio of 1:10 (v/v %) to the precursor was added into the gel solution. After 5 mins of manual stirring, the resulting mixture was ultrasonicated for 10 min at room temperature (23°C). In the next step, the mixture was put into a vacuum chamber to degas for 20 min, after which the CNC/PDMS mixture was cast onto a silicon (Si) mold with the bridge structure. In order to form a flat and smooth surface, the Si mold was placed onto a hotplate to let CNC/PDMS mixture disperse (flow) at room temperature for 5 mins, and the temperature was then increased to 80 °C for 30 min to complete the curing process. The samples for mechanical testing were also fabricated in the same way, with a different mold shape.
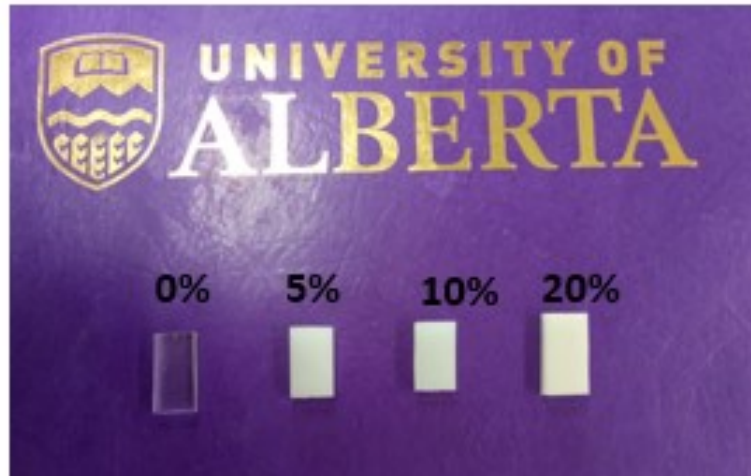
Figure 3-1: CNC/PDMS nanocomposite films with different weight ratio of CNC (0%; 5%; 10%; 20%).

3.2.3 Tensile measurement

The mechanical properties of CNC/PDMS nanocomposite films were measured by Instron 5943 Single Column Tabletop Testing Systems (Norwood, MA, USA) at room temperature using a 1 kN load cell. Following the ASTM D412 test standard, dumbbell shape samples, which have two large ends for clamping and a narrow testing section in the middle, were fabricated for testing. At first, the CNC/PDMS mixture was cast onto a three-layer metal mold to form a uniform dumbbell testing sample (Dimensions: thickness: 3 mm; length: 100 mm; width: 10 mm). The tensile test rate was performed at a rate of 5 mm/min; samples were strained until breaking. The extension of the tested region and the force sensed by the load cell were obtained from the raw data, and then were converted to strain and stress with respect to the initial sample dimensions. At least five specimens were tested for each type of samples. From the obtained stress–strain curves, the fracture stress (σ) and fracture strain (ε) at the breaking points were calculated. The Young's modulus (E) was calculated from the slope of the linear range (from 0% to 20% strain). As shown in the Fig. 3-2, the Instron 5943 Single Column Tabletop Testing Systems was used to perform the tensile test by clamping both sides of the dumbbell-shape sample.

Figure 3-2: the tensile test system used for studying the basic mechanical properties in the experiment.

3.2.4 Dynamic mechanical analysis

To study the viscoelastic properties of the CNC/PDMS nanocomposite films, dynamic mechanical analysis (DMA) measurements were carried out by using a PerkinElmer dynamic mechanical analyzer (DMA 8000) shown in Fig. 3-3. In order to ensure the consistency of the measurements, all samples for dynamic mechanical test were cut from the samples' clamped areas used in the tensile test, with dimensions of 16 mm x 10 mm x 2.8 mm. In single cantilever bending mode, the loss modulus (G") and storage modulus (G') as well as damping factor (tan delta) were measured at a frequency of 1 Hz under multiple strain conditions.
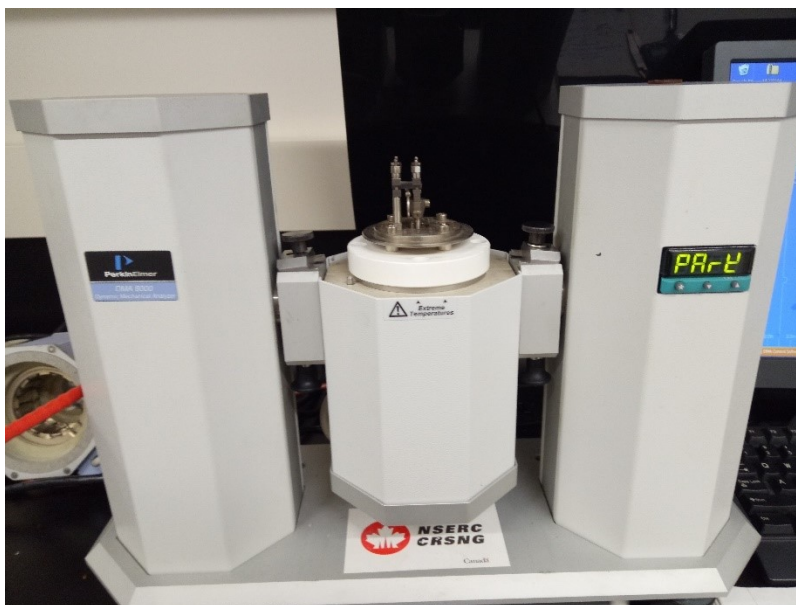
Figure 3-3: the DMA system used for studying the viscoelastic properties in the experiment.

3.3 Results and discussions

3.3.1 Mechanical property of CNC/PDMS nanocomposite film
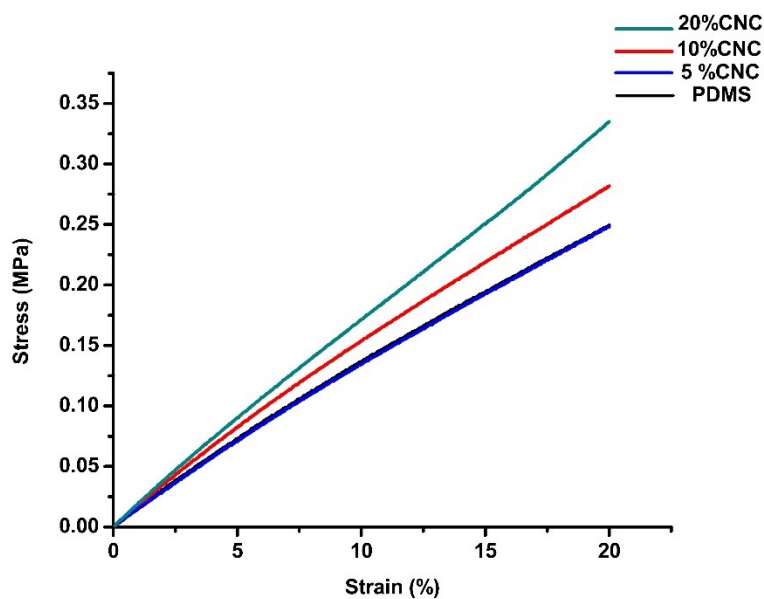
Figure 3-4: Representative stress– strain curves of nanocomposite films with different CNC concentrations.

Based on tensile measurements of each sample type, a characteristic tensile strain-stress curve is shown in Fig. 3-4, and a table of various mechanical parameters (Young's modulus, E, fracture stress, σ, and fracture strain, ε) is illustrated in Table 1.

Table 3-1. Mechanical Properties of CNC/PDMS nanocomposite films.

Sample	Young's Modulus (MPa)	Tensile strength (MPa)	Average ultimate tensile strain (%)
PDMS	1.02 ±0.06	4.2 ±0.06	200
5%CNC	1.15 ±0.11	3.7 ±0.05	170
10%CNC	1.42 ±0.09	2.9 ±0.12	150
20%CNC	1.87 ±0.07	2.6 ±0.05	100

The Young's modulus of each type of films was calculated using the equation: $E= \varepsilon/\sigma$. It is seen the Young's modulus for pure PDMS and 5% CNC/PDMS samples has similar values, while the 10% CNC/PDMS sample (red curve in Fig. 3-4) shows significant increase in Young's modulus. The modulus of the 20% CNC/PDMS sample is the largest, almost 2 times larger than that of pure PDMS sample. In addition to the well-known reinforcing effect of nanofillers on polymers, the hydroxyl groups of the CNCs may have a synergistic effect to improve the crosslinking of PDMS, which is the key factor leading to larger Young's modulus based on the theory in a previous report.[22] The mechanical characterizations confirm that such CNC fillers embedded in the polymer matrix have successfully combined both materials' advantages, which are the strong mechanical property from CNC and the flexible nature from PDMS.

3.3.2 Dynamic viscoelastic property

Most polymers, especially nanocomposite materials, are not purely elastic materials but also have a viscous component. When a strain is applied to the material, some of the energy

is stored and can be recovered as elastic energy, but some of the energy is dissipated within the material itself. One characteristic of a viscoelastic material is that there is a lag between the application or removal of a force and the resulting deformation (whereas purely elastic materials respond instantaneously). Therefore, viscoelastic property plays a significant role in the mechanical response of nanocomposite materials. In addition to tensile test, dynamic mechanical analysis (DMA) was performed to fully understand the viscoelastic properties of our CNC/PDMS nanocomposite materials. In the DMA test, a sinusoidal stress is applied to the test sample, and three characteristic parameters are measured: the storage modulus (G′), the loss modulus (G′′) and the delta (δ, also named damping factor). The storage modulus (G′) is the measure of the sample's elastic behaviour, and the loss modulus (G′′) represents the sample's viscous behaviour. The ratio of loss modulus to storage modulus is the tan delta, also named as damping, which is a measure of the energy dissipation in a material.

The dynamic stress and strain are defined as follows:

$$\sigma = \sigma_0 \sin(tw + \delta) \quad (1)$$

$$\varepsilon = \varepsilon_0 \sin(tw) \quad (2)$$

and measured G′ and G′′ as well as tan delta are defined as follows:

$$G' = \sigma_0/\varepsilon_0 \cos\delta \quad (3)$$

$$G'' = \sigma_0/\varepsilon_0 \sin\delta \quad (4)$$

$$\tan\delta = G''/G' \quad (5)$$

Where σ_0 and ε_0 are the largest amplitudes of stress and strain respectively; δ is the phase lag; w is the angular frequency of the sinusoidal stress; t is the time in the measurement.
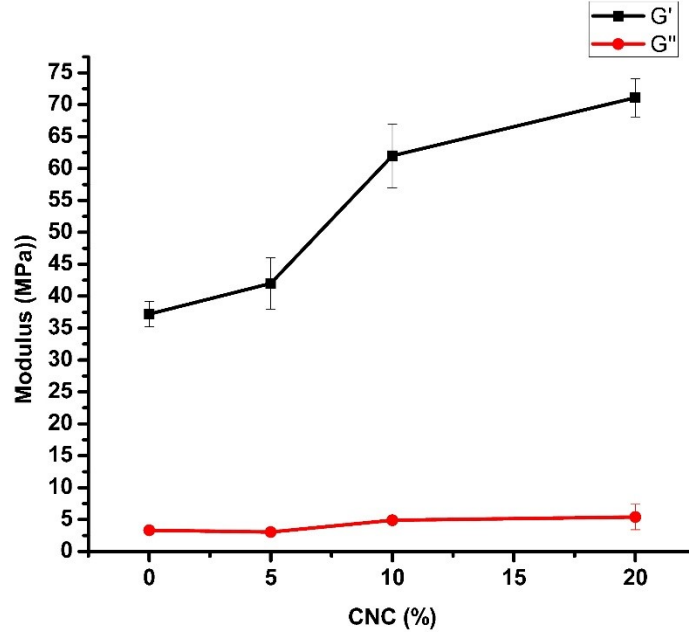
Figure 1-5: storage modulus (G') VS loss modulus(G")

As depicted in Fig. 3-5, the storage modulus (G') increases as CNC concentration increases from 0% to 20%. This trend agrees with observations in tensile test, which further confirm that adding CNC to PDMS has led to an extraordinary enhancement in elastic property (Young's modulus). However, from Fig. 3-5, there is only a small increase for the loss modulus(G"). Since the loss modulus indicates the energy dissipation (viscoelastic property) of composite materials, it is clear to say that with increasing concentration of CNC, the energy dissipation efficiency hasn't changed too much compared to storage modulus.
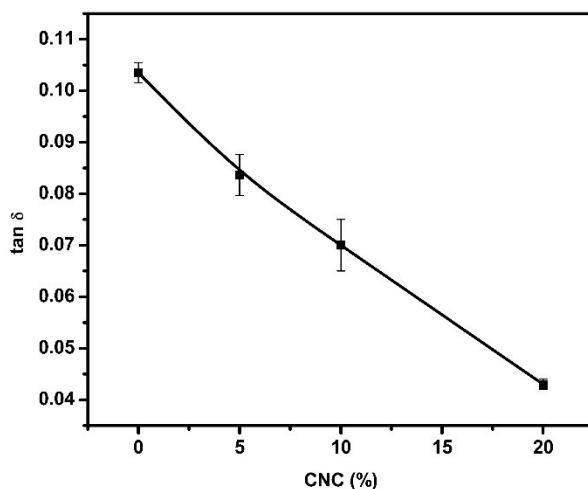
Figure 3-6: Loss factor tan delta as a function of CNC concentration.

As shown in equation (5), tan delta is calculated by the ratio of loss modulus G'' to storage modulus G'. Thus, like mentioned before, with increasing concentration of CNCs, larger storage modulus and almost unchanged loss modulus results in a decrease for tan delta, as shown in Fig. 3-6 reveals that the tan delta decreased almost in half with the increase in CNC content from 0% to 20%. Therefore, this trend of higher loading of CNC leading to smaller delta explains the faster response time of CNC/PDMS nanocomposite film in deformation. In order to visualize the influence of the change in delta, two preselected delta values were used to plot a schematic sin function wave as equation (1) and (2). As illustrated in Fig. 3-7, compared with pure PDMS sample (blue curve), 20% CNC/PDMS sample (black curve) has a smaller delta (phase lag), which means the resulted strain responds faster to the applied stress.
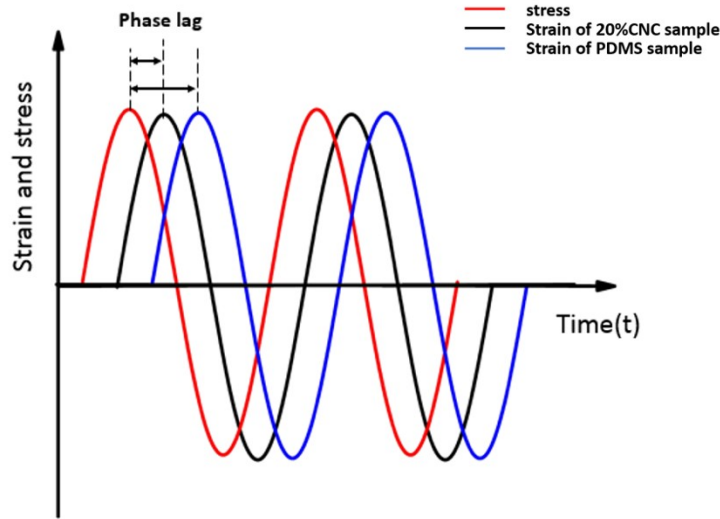
Figure 3-7: Schematic illustration of the influence of viscoelastic property on the strain responding to applied stress.

To directly measure the response time of MEM sensors employing CNC/PDMS nanocomposite materials, loading and unloading test was conducted using the compression mode of the Instron Testing System and an electrical measurement instrument (Keithley 2400). A constant pressure was applied to MEM sensors for about 1 s, then removed immediately. Fig. 3-8 shows the response of MEM sensors employing both pure PDMS and a CNC/PDMS composite. As shown in the figure, there is no observable difference for the rising time of MEM sensors when CNC is added, however, the relaxation time changes significantly. For the device with pure PDMS film (black curve), more than 0.2 s were needed to allow the current drop to minimum level (around 10-8 A), but for the device with CNC/PDMS nanocomposite, the relaxation takes less than 0.01 s, which is almost 20 times smaller than the original one. Combining the results from DMA, we conclude that the response time of our MEM sensors is greatly improved by adding CNC into PDMS to form nanocomposite materials.
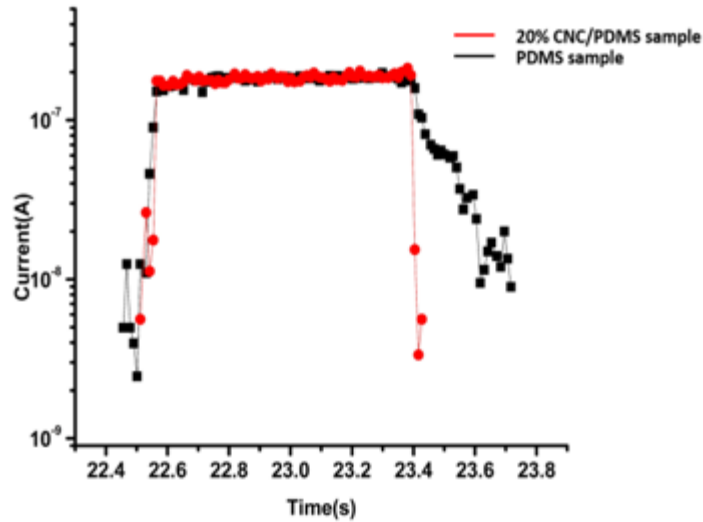
Figure 3-8: Loading and unloading test (red curve for 20% CNC/PDMS sample; black curve for PDMS sample).

3.3.3 Pressure response

In a digital MEM sensor, the conductivity threshold is regarded as a measure of a sensor's sensitivity. To study the influence of different concentrations of CNC on the conductivity threshold, the pressure test was performed for devices with the same PDMS structure but different CNC concentrations, as shown in Fig. 3-9. When the pressure increased to around 70 Pa, the top layer and bottom layer of the pure PDMS sample contacted completely. On the other hand, the threshold for nanocomposites samples with 5%, 10%, 20% (wt.%) CNC increased to 110 Pa, 190Pa, and 250 Pa, respectively which is 1.6-3.5 fold higher than pure PDMS sample. This phenomenon could be attributed to the increase in Young's modulus that results when CNC fillers are added to PDMS. Due to the change of Young's modulus, the threshold pressure changes accordingly. This provides a new method to adjust the sensitivity of MEM pressure sensors by modifying the concentration of the filler material. Although such increase in response time of MEM sensors by increasing CNC concentrations means the sensitivity of MEM sensors will decrease, the sensitivity can be

brought back to high precision levels by controlling the CNC/PDMS structures as shown in our previous report.[15]
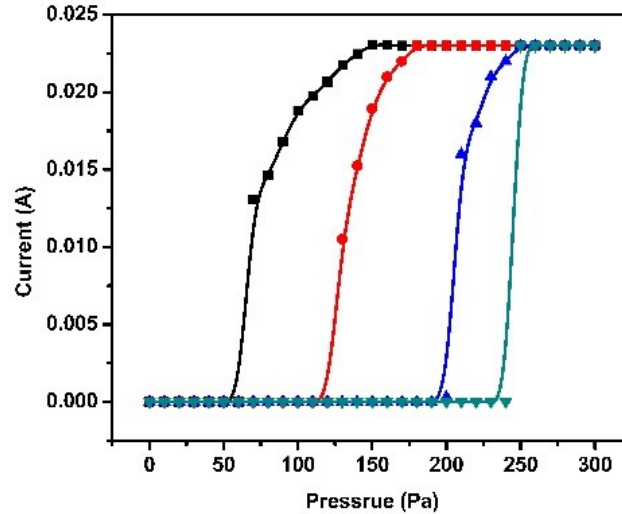
Figure 3-9: Conductivity threshold of CNC/PDMS nanocomposite pressure sensors, a voltage of 1 volt was applied for all devices. The black, red, blue and green curves represent the pure PDMS pressure sensor and nanocomposite sensors with 5%, 10%, 20% (wt.%) CNC, respectively.

3.3.4 Demonstration of integrated MEM sensors for blood pressure measurement

For the demonstration of fast response and high sensitivity of our pressure sensors, two bridges structured (38 μm & 48 μm pier height) CNC/PDMS (20wt.%) nanocomposite films were integrated onto a flexible polyimide substrate (DuPont, ®Kapton) to perform a blood pressure measurement. In our previous report,[15] we could only detect a simple pulse in a cardiac cycle due to the slow response of previous MEM sensors. Now, the MEM sensors can simultaneously detect multiple pressures and provide more information for analysis of cardiovascular signals.

The blood pressure at the human wrist, a radial artery pressure, consists of two waves: the incident wave generated by blood flow from the heart and the sum of reflected waves from the hand region and the lower body. In clinical non-invasive radial artery pressure analysis,[25] there are several commonly used parameters to present the condition of the radial artery stiffness. The first one is the time delay ΔT_{dvp}=t2-t1, where t1 and t2 represent the times for first and second peaks in radial artery pressure, and the second one is the reflection index (AKA stiffness index) RI=h/Δt, where h is the tester (e.g. patient) height and Δt is the difference between t1 and t2.
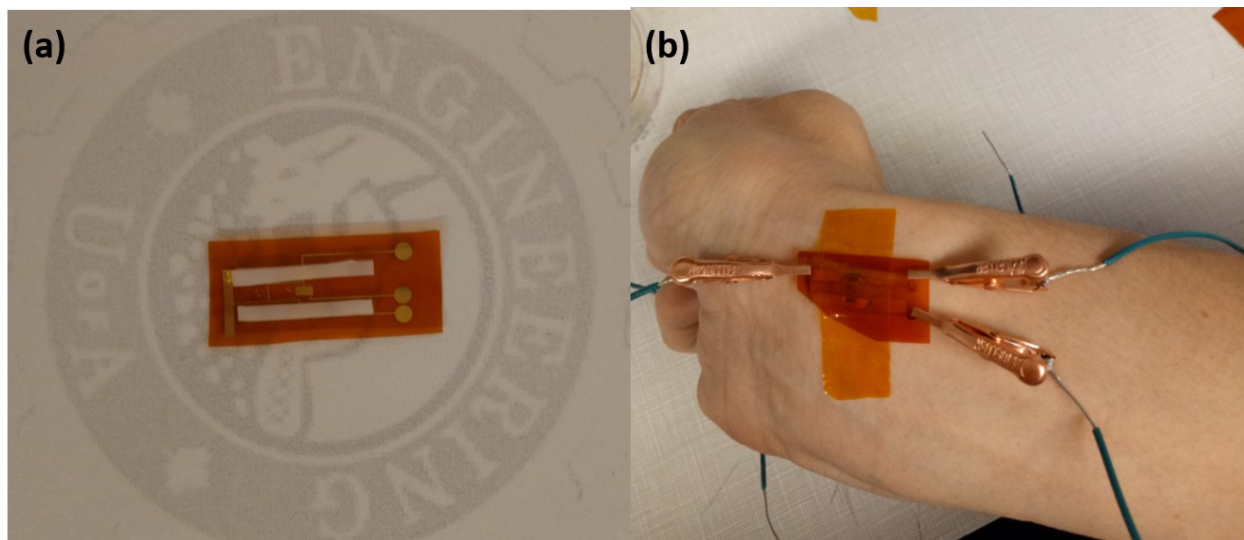
Figure 3-10: a) Integration of two devices with 48 μm and 38 μm pier height for blood pressure measurement. b) Photograph showing the MEM sensors attached directly above the radial artery of the wrist

Fig. 3-10 a) shows the integrated MEM sensors for blood pressure measurement; this device can be attached to the adult tester's wrist just above the radial artery as shown in Fig. 3-10 b). Fig. 3-11 a& b) show the real-time record of MEM sensors over several cardiac cycles, in which the red curve represents incident wave signal while the black curve means the sum of incident wave and reflected wave signals. As mentioned before, we can easily derive those characteristic parameters for arterial stiffness diagnosis, and obtained our test result, ΔT_{dvp}=300 ms and RI=5.8. According to the reported reference,[26] both of these

characteristic parameters fit to the typical values expected in the healthy range for the tester (a 24 years old adult male). This demonstration implies that our sensors are capable of resolving very small signal in radial artery pressure measurement. Furthermore, advantages of our MEM sensors such as low cost, easy fabrication, fast response, etc. will enable the potential of integrating our MEM sensors for future wearable systems.
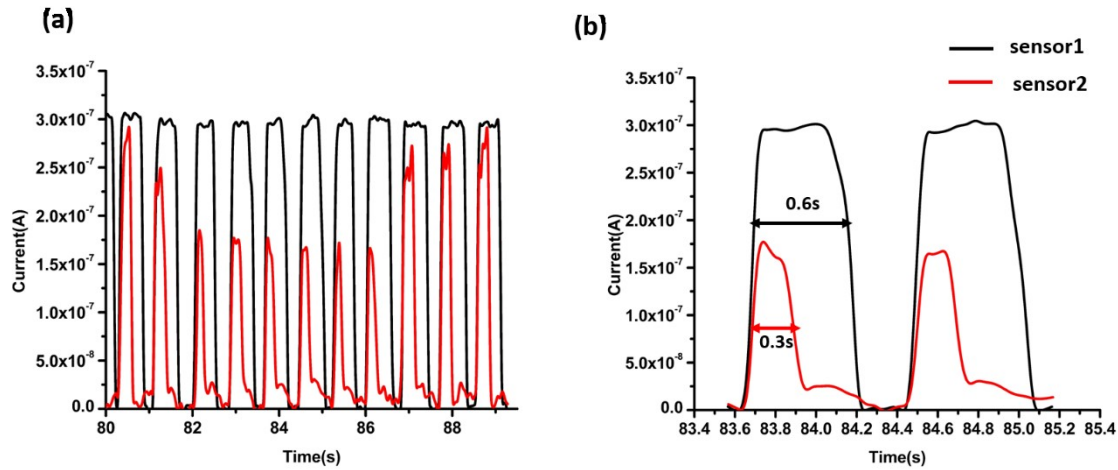
Figure 3-11: a) Measurement of the radial artery pressure change due to heart beating. b) A magnified picture of the device response in two cardiac cycles were picked to illustrate the calculation of t_1 and t_2.

Reference

1. W. Gao, S. Emaminejad, H. Y. Y. Nyein, S. Challa, K. Chen, A. Peck, H. M. Fahad, H. Ota, H. Shiraki, D. Kiriya, D.-H. Lien, G. A. Brooks, R. W. Davis and A. Javey, *Nature*, 2016, **529**, 509–514.

2. W. Honda, S. Harada, T. Arie, S. Akita and K. Takei, *Adv. Funct. Mater.*, 2014, **24**, 3299–3304.

3. D. J. Lipomi, M. Vosgueritchian, B. C.-K. Tee, S. L. Hellstrom, J. A. Lee, C. H. Fox and Z. Bao, *Nat. Nanotechnol.*, 2011, **6**, 788–792.

4. L. Y. Shao, A. Laronche, M. Smietana, P. Mikulic, W. J. Bock and J. Albert, *Opt. Commun.*, 2010, **283**, 2690–2694.

5. L. K. Simone, E. Elovic, U. Kalambur and D. Kamper, in *Conference proceedings : Annual International Conference of the IEEE Engineering in Medicine and Biology Society. IEEE Engineering in Medicine and Biology Society. Conference*, 2004, vol. 7, pp. 4791–4794.

6. E. Biddiss and T. Chau, *Med. Eng. Phys.*, 2006, **28**, 568–578.

7. Kenry, J. C. Yeo and C. T. Lim, *Microsystems Nanoeng.*, 2016, **2**, 16043.

8. D. J. Cohen, D. Mitra, K. Peterson and M. M. Maharbiz, *Nano Lett.*, 2012, **12**, 1821–1825.

9. T. Yamada, Y. Hayamizu, Y. Yamamoto, Y. Yomogida, A. Izadi-Najafabadi, D. N. Futaba and K. Hata, *Nat. Nanotechnol.*, 2011, **6**, 296–301.

10. K. S. Kim, Y. Zhao, H. Jang, S. Y. Lee, J. M. Kim, K. S. Kim, J.-H. Ahn, P. Kim, J.-Y. Choi and B. H. Hong, *Nature*, 2009, **457**, 706–710.

11. J. Wang, J. Jiu, M. Nogi, T. Sugahara, S. Nagao, H. Koga, P. He and K. Suganuma, *Nanoscale*, 2015, **7**, 2926–2932.

12. J. Lee, S. Kim, J. Lee, D. Yang, B. C. Park, S. Ryu and I. Park, *Nanoscale*, 2014, **6**, 11932–11939.

13. B. P. Timko, T. Dvir and D. S. Kohane, *Adv. Mater.*, 2010, 22, 4925–4943.

14. L. Meng, S. Fan, S. M. Mahpeykar and X. Wang, *Nanoscale*, 2017, **9**, 1257–1262.

15. L. Meng, S. M. Mahpeykar, Q. Xiong, B. Ahvazi and X. Wang, *RSC Adv.*, 2016, **6**, 85427–85433.

16. D. Chen, F. Chen, X. Hu, H. Zhang, X. Yin and Y. Zhou, *Compos. Sci. Technol.*, 2015, **117**, 307–314.

17. a. M. Stricher, R. G. Rinaldi, C. Barrès, F. Ganachaud and L. Chazeau, *RSC Adv.*, 2015, **5**, 53713–53725.

18. S. C. B. Mannsfeld, B. C.-K. Tee, R. M. Stoltenberg, C. V. H.-H. Chen, S. Barman, B. V. O.

Muir, A. N. Sokolov, C. Reese and Z. Bao, *Nat. Mater.*, 2010, **9**, 859–64.

19. J. Yang, J. Chen, Y. Su, Q. Jing, Z. Li, F. Yi, X. Wen, Z. Wang and Z. L. Wang, *Adv. Mater.*, 2015, **27**, 1316–1326.

20. G. Schwartz, B. C.-K. Tee, J. Mei, A. L. Appleton, D. H. Kim, H. Wang and Z. Bao, *Nat. Commun.*, 2013, **4**, 1859.

21. J. George and S. N. Sabapathi, *Nanotechnol. Sci. Appl.*, 2015, **8**, 45–54.

22. D. Ponnamma, K. K. Sadasivuni, M. Strankowski, Q. Guo and S. Thomas, *Soft Matter*, 2013, **9**, 10343–10353.

23. K. K. Sadasivuni, A. Kafy, L. Zhai, H. U. Ko, S. Mun and J. Kim, *Small*, 2015, **11**, 994–1002.

24. A. Pei, J. M. Malho, J. Ruokolainen, Q. Zhou and L. A. Berglund, *Macromolecules*, 2011, **44**, 4422–4427.

25. W. W. Nichols, *Am. J. Hypertens.*, 2005, **18**, 3–10.

26. S. C. Millasseau, R. P. Kelly, J. M. Ritter and P. J. Chowienczyk, *Clin. Sci. (Lond).*, 2002, **103**, 371–377.

Chapter 4. Polymer microelectromechanical systems (MEMS) for integrated flexible sensors

4.1 Introduction

Silicon based MEMS devices have been fabricated for pressure sensors,[1] digital micromirrors,[2] nozzles of inkjet printers,[3] accelerometers,[4] gyroscopes,[5] etc. with broad applications in automobiles, medical equipment, and consumer electronics.[6] The rapid adoption of these MEMS devices benefits from the advantages of MEMS in high sensitivity, ease of integration, complex functionalities, and efficiency in power utilization and manufacturing. There are more opportunities of MEMS sensors and actuators, as building blocks of sensing and communication hardware, for internet-of-things applications in the future. However, these silicon MEMS devices are not truly flexible. While microstructured polymers can be employed as functional elements for flexible MEMS sensors.   Flexible strain and pressure sensors are of interest for academia and industry for their broad applications in wearable devices,[7] medical instruments,[8] robotics,[9] and e-skin products.[10] Most of previously reported strain and pressure sensors focus on the development of new materials, including but not limited to carbon nanotubes,[11] graphene and 2D semiconductors,[12, 13] metal and semiconductor nanowires[14] and nanoparticles,[15] and polymers.[16] These sensors probe capacitance and/or resistance changes of materials under applied pressure/strain. Besides above-mentioned works on exploring new materials, novel device architectures can also bring a variety of functions to flexible strain and pressure sensors. For example, we just reported microelectromechanical sensors like mechanical switches for hand gesture detection and heart rate monitoring.[17] Although individual sensors only output digital signals, integration of multiple sensors with various

sensitivities can achieve similar functions as provided by regular sensors with analog signal output.

Here we propose an approach to directly integrate microelectromechanical sensors using polymer MEMS. In this method, three microelectromechanical sensors were fabricated simultaneously using a PDMS based MEMS on the polyimide substrate. The engineered MEMS device with three distinct sensitivities in bending can be fabricated for controlling robotic arms. This MEMS device can also be used as the pressure sensor when handle physical objects. The PDMS MEMS, compared to widely used silicon MEMS, inherits flexible and stretchable natures from polymer materials, and is used to build truly flexible sensors on polymer substrates. Our polymer MEMS devices have the potential to be conformally integrated on curved surfaces for future applications in wearable technologies.

4.2 Experimental details

4.2.1 material

FX-900 photopolymer film was used as the photoresist in photolithography and it was purchased from DuPontTM. Typical thickness of FX-900 photopolymer films ranges from 20 μm to 62 μm and the exposure dose in photolithography varies from 35 mJ/cm2 to 155 mJ/cm2 for different thickness of photoresist. Sylgard 184 silicone elastomer kit, which includes the cross-linker and polydimethylsiloxane (PDMS) elastomer, was purchased from Dow Corning for preparing PDMS MEMS.

4.2.2 Preparation of upper layer mold

As shown in the in Fig. 1, a soft-lithography-like method was used to fabricate the mold for the multilayer structure. In the first step (Fig. 4-1 Step 1), a piranha-cleaned 4-inch silicon

wafer was prepared as the substrate for dry photoresist lamination. It's worth noticing that the adhesion of FX-900 dry photoresist to the silicon wafer is stronger compared with other metal substrates18 and the PDMS peel-off process can be easily performed on silicon wafer.

Next, dry photoresist layer with thickness of 30 μm was laminated onto the substrate by a dry-film laminator (Akiles ProLam 6R) (roll laminator temperature set to 110˚C), then UV-lithography was performed for 2 s to build a base circular pattern with 8000 μm in diameter (Fig. 4-1 Step 2). Here, it is necessary to define alignment marks in this layer to which subsequent layers can be aligned precisely and properly. In order to obtain better flatness and stronger adhesion for each layer, a post exposure baked (PEB) process was required after exposure step. In this step, 110ºC for 3 mins was set for standard PEB parameters. According to different thickness of photoresist films, PEB time, temperature, and the cooling down time to room temperature have to be customized to guarantee that the mask layout can be perfectly retrieved in the photolithography process. If the UV exposure and PEB process are ideal, the exposed areas of photoresist will be noticeably darkened which makes it readily visible for further alignment, otherwise further lamination would be difficult to be performed. Development was typically conducted in standard sodium carbonate solutions. Development time was adjusted according to the thickness of photoresist films and critical feature sizes. Smaller features will require longer time to be fully developed. For example, the developing time was 3 mins for first layer as shown in Fig. 1 Step 3, but the development time of the 2nd and 3rd layers are 5 mins and 10 mins.

For the second layer, another FX-900 dry photopolymer film with the same thickness was laminated onto the substrate and pattern through the second photomask with 8000 μm in diameter for the base circular and 800 μm in diameter for the circular hole (Fig. 4-1 Step

4). The developing time was extended to 5 mins to obtain better lithography results (Fig. 1 Step 5). The process to form the last layer was almost same as the formal steps. However, the parameters for lamination and pattern process require adjustments. According to the optimized experimental results, for the third layer, the lamination temperature was increased to 130°C and the development process was extended to 10 mins with agitation (Fig. 4-1 Step 6 & 7). In summary, the key parameters like lamination temperature, developing time for each step were listed in Table 1.
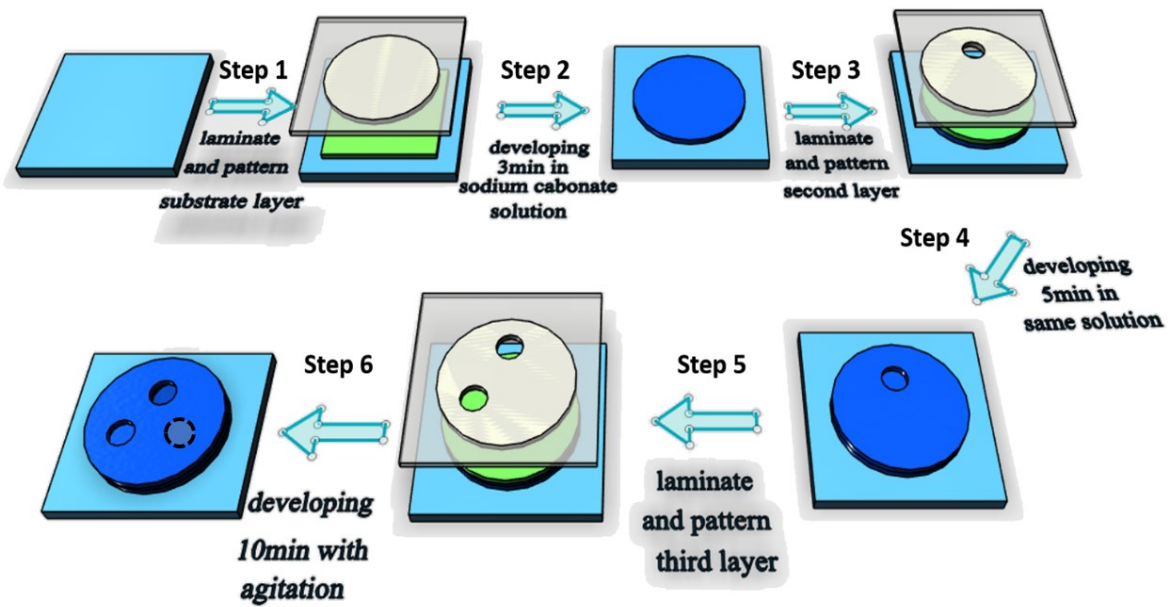

Figure 4-2: Basic fabrication process for multilayer-structured mold

Table 4-1: Key parameters in the fabrication process

Layer/Parameter	Lamination temperature	Exposure time	Development time	Agitation
1st layer	110 ˚C	2 s	3 min	Not required
2nd layer	120 ˚C	2 s	5 min	Not required
3rd layer	130 ˚C	2 s	10 min	Needed

4.2.3 Pressure sensor fabrication

After obtaining the ideal upper layer mold, we casted the mixture of PDMS base and crosslinker (Dow Corning Sylgard 184 kit) in ration of 10:1 onto the patterned mold for fabricating the upper layer. In order to assure the flatness of the film, such process was conducted in the spin-coating station with a spin speed of 200 rpm. Then the mold was put onto hotplate at $80 C°$ for 30 mins to make PDMS totally solidified.

We used the lift-off photolithography process to fabricate the bottom electrode on the polyimide film (DuPont, Kapton), Then 60 nm gold layer with 10 nm chromium adhesion layer was sputtered on the Kapton film and upper PDMS circular structure. At last, same bonding process was used the same bonding method in our previous work17 to realize the tight attachment of upper PDMS microstructures on the bottom polyimide layer. Fig. 2a) illustrates the structure for upper PDMS layer and bottom electrodes. The critical step in this process is the alignment between upper layer and bottom layer, because if upper layer and bottom layer are not aligned properly, it may influence the performance of our devices.

4.2.4 Characterizations of polymer MEMS devices

In our experiments, we characterized the performance of polymer MEMS devices from two aspects: bending-strain test and pressure-force test. In the pressure test, the sensor was attached to the stable stand in Instron 5943 Single Column Tabletop Testing Systems (Norwiod, Ma, USA), under compression mode, and a controllable force was applied by connecting a flat-top cylinder to the force gauge with a loading speed of 1 mm/min. While in the strain test, we used the double-sided tape to attach our devices on the steel blocks with different radii. The electrical signals from polymer MEMS devices was recorded in real time using both source-meters (Keithley 2400) and a data acquisition box (DAQ USB-6008, National Instruments), and the measurement system was controlled by Labview.

4.3 Results and discussions

4.3.1 Strain& Pressure test

Fig. 4-2b) shows the electrical current vs. strain curves for the typical polymer MEMS integrated flexible sensors. In this bending strain test, when our device was conformally attached onto steel blocks with different radii, it was stretched to certain strains. When the radius becomes smaller, the corresponding strain was bigger. The top pillar in PDMS MEMS will connect with the bottom substrate when the strain reaches to a certain value. As shown in Fig. 4-2b), the black, red, blue curves represent electrical signals from sensors with cavity height (distance between pillar and bottom substrate at original states) of 38 μm, 76 μm and 114 μm, respectively. It is clearly noticed that with the changing in cavity height, the threshold strains of individual sensors to trigger connection vary relatively. For the first pillar with a cavity height of 38 μm, the threshold strain is small – only 0.083%. For the other two cavities with the cavity height of 78 μm and 114 μm, the threshold strains are 0.13% and 1.00%. Although our devices cannot monitor continuous strain changes like typical strain sensors, thanks to large threshold differences among individual pillars, our devices are capable of detecting strains with orders of magnitude changes. For many practical cases, the accurate monitoring of applied strains is not necessary, on the contrary, the measurement of several key points in the applied strains are desired, like the strain alarm for flexible electronics. By engineering the pillar height in PDMS MEMS, one can easily design integrated flexible sensors to achieve different strain detection thresholds for various applications.
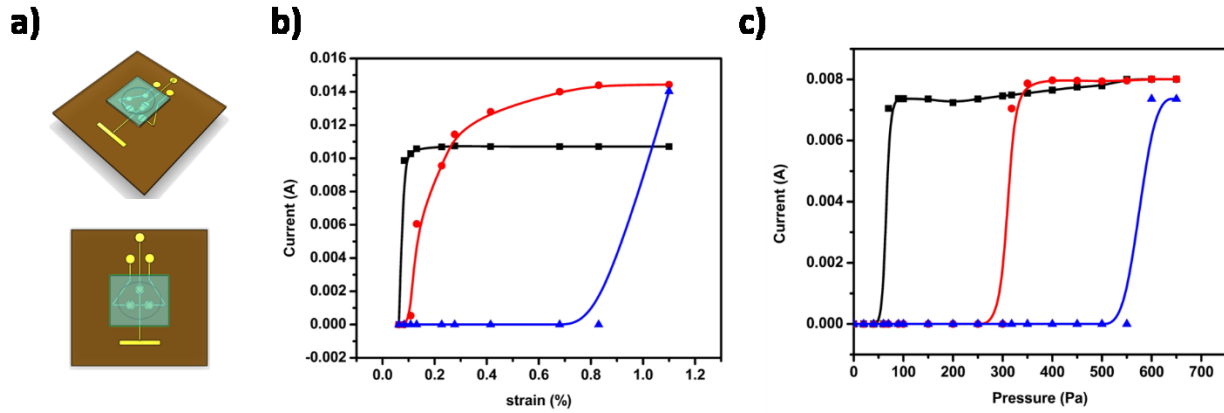
Figure 4-3: Characterizations of polymer MEMS devices. a) Structure of the polymer MEMS device integrated with three sensors. Bottom one is the top view of the device. b) Currents flowing through the device when different strains applied to the substrate. In this graph, the blue, black and red curves represent sensors with 114 μm, 76 μm and 38 μm cavity height. c) Currents flowing through the device when different pressures applied to the device, a voltage of 1 volt was applied for all sensors. The black, red, blue and green curves represent the sensors with 114 μm, 76 μm and 38 μm cavity height.

As shown in Fig. 4-2c), the black, red, blue curves represent cavity height of 38 μm, 76 μm and 114 μm for three integrated flexible sensors. Here, conductive threshold is used to define the pressure sensitivity of our sensors. It is obvious to see that when the pressure increases to 60 Pa, the first pillar contacts the bottom layer and one sensor starts to output electrical signals. With the pressure increasing to 250 Pa, the second pillar connects with the bottom layer. At last, while the pressure reaches to 510 Pa, all of the top layers connect with the bottom substrate. Therefore, the integrated three pressure sensors in a polymer MEMS device have distinct pressure thresholds which represent different sensitivities to the applied pressure, as shown in Fig. 4-2b). Since the cavity height of each sensor is controllable, the polymer MEMS device is feasible to monitor different scale of applied pressures as needed.

4.3.2 Applications of polymer MEMS flexible sensors

According to the strain and pressure test in the above-mentioned section, our polymer MEMS flexible sensors show the capability to work in two modes: bending and pressing.

To demonstrate our sensors for practical use, here we apply our sensors as finger controller for robotic arms and pressure detector for gripping force.

***Finger controller for robotic arms*:** As discussed above, the polymer MEMS device could distinguish three different bending strains, therefore, we apply it to detect the finger movement which has the potential to control robotic arms. In Fig. 4-3, one polymer MEMS device was attached to the index finger at the joint. For illustration, a virtual robotic arm was created on the display by the software - Labview. In the experiment, we only applied one polymer MEMS device onto the mid-joint for demonstration. When the finger bends slightly (reach to the first threshold), the robotic arm will capture this motion and bend to a certain degree at the same time (Fig. 4-3b). Since the MEMS device has three strain thresholds, further finger bending led the other two upper electrodes from second pillar and cavity's top layer to contact with bottom electrodes. In the meantime, the robotic arm could bend correspondingly (Fig. 4-3c, d). In the supplementary information, a video was shown for this demonstration. It is clearly seen in the video that the when finger bent to different angles, our polymer MEMS sensor had relevant responses which was confirmed by the virtual robotic arm animation. It's also noted from the video that when we released the finger, the recover process was swift and stable with all three compressed areas back to original states immediately (Fig. 4-3a). The result demonstrates that our sensor can be applied to detect the finger motions. Furthermore, in this demonstration, only one sensor was used for one finger joint, but as the robotic arm showed, for our finger, there are three joints for each finger. So, in the future work, we are planning to integrate three polymer MEMS sensors in each finger, after that, capturing any kind of finger motions or combinations will be achievable and promising at that time.
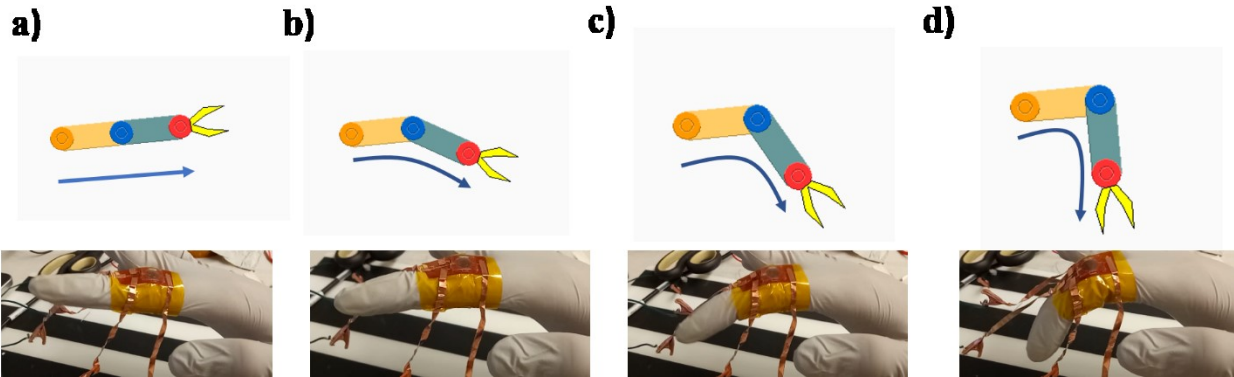
Figure 4-4: Demonstration of the polymer MEMS device on the human finger as bending sensors. A virtual robot arm was used to simulate the finger bending motion.

***Pressure sensors for detecting fingertip gripping force*:** Another potential application of our polymer MEMS device is to integrate it onto the fingertip as the pressure sensor for monitoring griping force in handling physical objects. In this demonstration, a quail egg was used as our test subject. As shown in Fig. 4-4 Section I, when little gripping force (or pressure) was applied, all three upper pillars in polymer MEMS remain no connection with the bottom substrate. After gripping force increased slightly, the first pillar connected to the bottom layer as shown in Section II and Sensor 1 outputted electrical signals. With the further increase of gripping force, both first and second pillars contacted the bottom layer (Section III), and we observed signals from both Sensor 1 and Sensor 2. In the end, when very large gripping force was applied (Section IV), all three sensors output electrical signals. Finally, the egg was crashed, the deformation of polymer MEMS subsequently came back to its starting state (Section V), and the electrical signals of all sensors went down to zero, similar to these in Section I. According to this demonstration, our polymer MEMS devices have the potential to be used as pressure alarms in robotics and prosthetics. For example, our sensors could sense different levels of pressures when robots grabbing physical objects in manufactory. If the pressure reaches to the maximum level, it will set an alarm for notification to avoid machine damage to products.
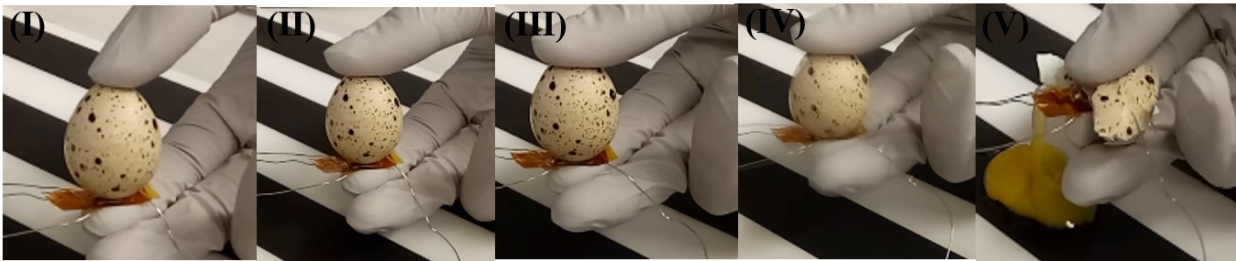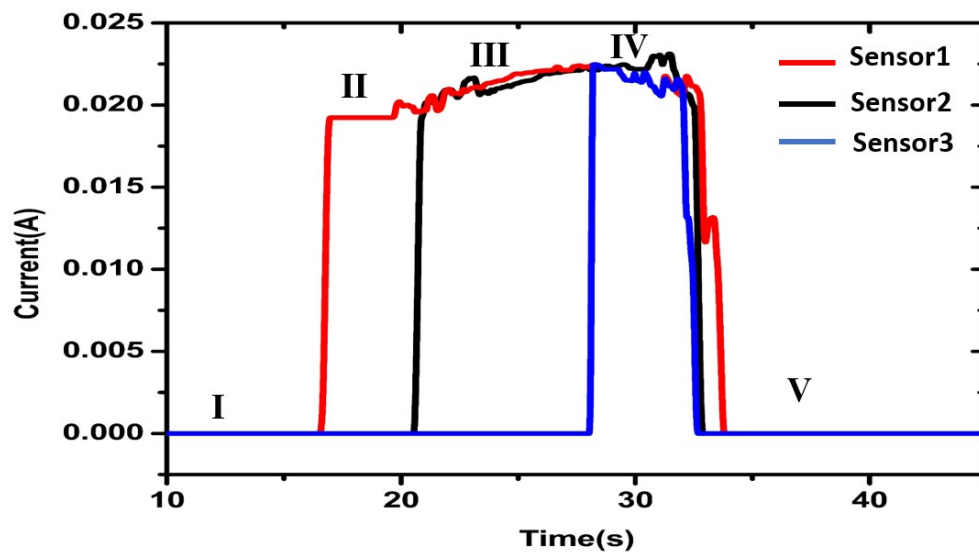
Figure 4-5: Application of the polymer MEMS device for monitoring pressures in gripping a quail egg.

Reference:

1. N. Marsi, B. Majlis, A. Hamzah and F. Mohd-Yasin, *Microsyst Technol,* 2015, DOI: 10.1007/s00542-014-2353-y.

2. P. EAKKACHAI, K. Rabenorosoa, M. Rakotondrabe and N. Andreff, *Micromachines,* 2016, .

3. Kyoung Il Lee, Byungjik Lim, Se Wook Oh, Seong Hyun Kim, Churl Seung Lee, Jin Woo Cho and Yongtaek Hong, *MEMSYS,* 2014, DOI: 10.1109/MEMSYS.2014.6765803.

4. R. Lawes, *MEMS Cost Analysis*, Pan Stanford, Singapore, 2016.

5. Yongcun Hao, Weizheng Yuan, Jianbing Xie and Honglong Chang, *The Institute of Electrical and Electronics Engineers, Inc. (IEEE) Conference Proceedings,* Jan 1, 2016, .

6. Z. Fekete, *Sensors and Actuators B: Chemical,* 2015, DOI: 10.1016/j.snb.2015.03.055.

7. B. C. K. Tee, A. Chortos, R. R. Dunn, G. Schwartz, E. Eason and Z. Bao, *Advanced Functional Materials,* 2014, **24**, 5427-5434.

8. Y. Khan, A. E. Ostfeld, C. M. Lochner, A. Pierre and A. C. Arias, *Advanced Materials,* 2016, DOI: 10.1002/adma.201504366.

9. D. Y. Choi, M. H. Kim, Y. S. Oh, S. Jung, J. H. Jung, H. J. Sung, H. W. Lee and H. M. Lee, *Chemicals & Chemistry,* 2017.

10. S. Harada, K. Kanao, Y. Yamamoto, T. Arie, S. Akita and K. Takei, *ACS nano,* 2014, .

11. I. Kang, M. J. Schulz, J. H. Kim, V. Shanov and D. Shi, *Smart Materials and Structures,* 2006, DOI: 10.1088/0964-1726/15/3/009.

12. Y. Wang, R. Yang, Z. Shi, L. Zhang, D. Shi, E. Wang and G. Zhang, *ACS nano,* 2011, .

13. L. Chiesi, P. Kejik, B. Janossy and R. S. Popovic, *Sensors and Actuators A: Physical,* 2000, DOI: 10.1016/S0924-4247(99)00360-X.

14. S. Yao and Y. Zhu, *nanoscale*, Royal Society of Chemistry, 2014.

15. J. Lee, S. Kim, J. Lee, D. Yang, B. Chon Park, S. Ryu and I. Park, *nanoscale*, Royal Society of Chemistry, 2014.

16. M. Knite, V. Teteris, A. Kiploka and J. Kaupuzs, *Sensors and Actuators A: Physical,* 2004, DOI: 10.1016/j.sna.2003.08.006.

17. L. Meng, S. Fan, S. Milad Mahpeykar and X. Wang, *nanoscale*, Royal Society of Chemistry, 2013.

18. Data sheet and processing information, DuPont™ Riston® Special FX900 Series.

Chapter 5. Conclusions and Future works

5.1 Conclusions

This chapter concludes the experimental results and analysis about our new concept, the digital strain/pressure sensors, and its applications in wearable devices. Based on the insulating-to-conducting transition of devices through mechanical switching, we proposed a new concept – the digital strain/pressure sensor, and applied it for wearable technologies. In order to improve the performance of our sensors, the method of employing eco-friendly nanomaterials - cellulose nanocrystals to improve response time (more than one order of magnitude) of the MEM sensors is provided. Finally, by redesigning the device architecture, a single device with three different levels of sensitivities has been demonstrated for detecting strain and pressure signals.

Digital microelectromechanical (MEM) sensors on flexible substrates

We proposed the concept of digital MEM sensor which opens a new path in force detection with higher stability and calibration-free property. We also demonstrated a design of engineered PDMS bridge structures. Relying on the simple structure and working mechanism, this kind of senor could work stably after more than 10000 cycles of loading and unloading test. The results showed that our devices have better stability and as a proof of concept, this device was applied to monitor finger bending and heart rate.

Improved response time of flexible microelectromechanical sensors employing eco-friendly nanomaterials

We presented an easy approach to obtain fast-response nanocomposite materials by adding CNC (an environment-friendly material with good mechanical property) to PDMS. Throughout regular tensile test and dynamic mechanical analysis, mechanical reinforcement of nanocomposite

materials is observed and attributed to the interaction of PDMS and CNC, as well as the material reinforcement of CNC itself. The dramatically improved response time was observed in DMA test and then confirmed in loading and unloading test. Besides the advantages of MEM sensors like higher stability and calibration-free property, such improvement of response time enables our sensors to detect real-time pulses in radial artery pressures. With proper integration of flexible MEM sensors employing engineered PDMS bridge structures and CNC concentrations, our devices enable continuous monitoring of heart rate and complex cardiovascular signals using pressure sensors for future wearable sensing platforms.

Polymer microelectromechanical systems (MEMS) for integrated flexible sensors

We demonstrated a new method to fabricate polymer MEMS devices using dry- photoresist lamination, and have integrated three electrical sensors (the area of 50 mm2) into one device for strain and pressure detection. Compared with standard polymer MEMS fabrication using SU-8 and other liquid photoresists, using dry film photoresist is attractive for rapid prototyping. Our devices were characterized in bending and pressing tests, and have the potential to be mechanically robust and reliability in life cycle measurement. We also demonstrated two practical applications of our devices, from virtual control of robotic arms to pressure monitoring in handling physical objects. By engineering the PDMS circular structures, our polymer MEMS devices have great potential to be applied in skin-like wearable and stretchable electronics.

5.2 Future works

The fabrication and characterization of our digital pressure/strain sensor are successfully presented in this thesis. In the meanwhile, simple practical applications of these sensors have been demonstrated. According to above-mentioned works, our sensors show great potential in

wearable devices, however, there are still certain limitations that need to be solved before commercial use. Some follow-up works are proposed below for practical use of our sensors.

5.2.1 Complete sensing system

According to previous demonstrated applications, our sensor could be applied to monitor the finger bending and blood pressures. However, these simple demonstrations are limited to a lab environment and a complete sensing system is required for practical use. For example, more pressure/strain sensors (i.e. 5 to 10 devices) could be integrated onto a glove to probe the motion of each fingers and the hand. As we mentioned in the introduction section, an integrated sensing system with complex functionalities is appreciated for practical use, so there is a great potential to integrate our pressure/strain sensors with other sensors like temperature senors into a complete sensing system in the future.

5.2.2 Optimization of fabrication process

As we mentioned in the chapter 4, the fabrication process for multilayer structures could be further optimized to improve the sensitivity and repeatability of our sensors. As for now, there are a few defects and gaps observed in the fabricated structure which is mainly caused by improper alignment between each layer. Thus, better design of alignment marks is needed for getting better structures and device performance.

5.2.3 Improvement of external connections

For now, our device is still facing the problem of using unreliable connections in the measurement. The way of using wires to connect sensors with the power source or test equipment brings a lot of troubles in measurement. In order to achieve a reliable sensing system, much more attention has to be paid to the design and fabrication of the external connections between different electronic components in the sensing system. Furthermore, developing wireless devices is also a trend in

wearable technologies, so build up a wireless sensing system could be the best solution to this problem.

Reference

1. A. M. Stricher, R. G. Rinaldi, C. Barrès, F. Ganachaud and L. Chazeau, RSC Adv., 2015, **5**, 53713–53725.

2. A. Nathan, Ahnood A, Cole M T, et al. Proceedings of the IEEE, 2012, **100** (Special Centennial Issue), 1486-1517.

3. A. Pei, J. M. Malho, J. Ruokolainen, Q. Zhou and L. A. Berglund, Macromolecules, 2011, **44**, 4422-4427.

4. B. C. K. Tee, A. Chortos, R. R. Dunn, G. Schwartz, E. Eason and Z. Bao, Advanced Functional Materials, 2014, **24**, 5427-5434.

5. B. P. Timko, T. Dvir and D. S. Kohane, Adv. Mater., 2010, **22**, 4925–4943.

6. C. L. Choong, M. B. Shim, B. S. Lee, S. Jeon, D. S. Ko, T. H. Kang, J. Bae, S. H. Lee, K. E. Byun, J. Im, Y. J. Jeong, C. E. Park, J. J. Park and U. I. Chung, Advanced Materials, 2014, **26**, 3451-3458.

7. C. Liu and J. Choi, Journal of Micromechanics and Microengineering, 2009, **19**, 085019

8. D. Chen, F. Chen, X. Hu, H. Zhang, X. Yin and Y. Zhou, Compos. Sci. Technol., 2015, **117**, 307–314.

9. D. Clark, Graphic Communication, 2010.

10. D. J. Cohen, D. Mitra, K. Peterson and M. M. Maharbiz, Nano Lett., 2012, **12**, 1821–1825.

11. D. J. Lipomi, M. Vosgueritchian, B. C. -. Tee, S. L. Hellstrom, J. A. Lee, C. H. Fox and Z. Bao, Nat Nano, 2011, **6**, 788-792.

12. D. P. J. Cotton, P. H. Chappell, A. Cranny, N. M. White and S. P. Beeby, IEEE sensors journal, 2007, **7**, 752-761.

13. D. Ponnamma, K. K. Sadasivuni, M. Strankowski, Q. Guo and S. Thomas, Soft Matter, 2013, **9**, 10343–10353.

14. D. Y. Choi, M. H. Kim, Y. S. Oh, S. Jung, J. H. Jung, H. J. Sung, H. W. Lee and H. M. Lee, Chemicals & Chemistry, 2017, **9**, 1770-1780.

15. Data sheet and processing information, DuPont™ Riston® Special FX900 Series.

16. E. Biddiss and T. Chau, Med. Eng. Phys, 2006, **28**, 568–578.

17. F. A. M. Davide, C. Di Natale and A. D'Amico, Sensors and Actuators: B. Chemical, 1993, **13**, 327-332.

18. G. R. Witt, Thin Solid Films, 1974, **22**, 133-156.

19. G. Schwartz, B. C.-K. Tee, J. Mei, A. L. Appleton, D. H. Kim, H. Wang and Z. Bao, Nat. Commun., 2013, **4**, 1859.

20. G. T. Hwang, M. Byun, C. K. Jeong and K. J. Lee, Advanced Healthcare Materials, 2015, **4**, 646-658.

21. H. Gleskova, S. Wagner, W. Soboyejo and Z. Suo, Journal of Applied Physics, 2002, **92**, 6224-6229.

22. H. Huang and F. Spaepen, Acta Materialia, 2000, **48**, 3261-3269.

23. H. Liang, Q. Guan, Z. Zhu, L. Song, H. Yao, X. Lei and S. Yu, NPG Asia Materials, 2012, **4**, 19.

24. Hemtej Gullapalli, Venkata S M Vemuru, Ashavani Kumar, Andres Botello-Mendez, Robert Vajtai, Mauricio Terrones, Satish Nagarajaiah and Pulickel M Ajayan, Small (Weinheim an der Bergstrasse, Germany), 2010, **6**, 1641-1646.

25. I. Kang, M. J. Schulz, J. H. Kim, V. Shanov and D. Shi, Smart Materials and Structures, 2006, **15**, 737.

26. J. George and S. N. Sabapathi, Nanotechnol. Sci. Appl., 2015, **8**, 45–54.

27. J. Kim, M. Lee, H. J. Shim, R. Ghaffari, H. R. Cho, D. Son, Y. H. Jung, M. Soh, C. Choi, S. Jung, K. Chu, D. Jeon, S. Lee, J. H. Kim, S. H. Choi, T. Hyeon and D. Kim, Nature Communications, 2014, **5**, 5747.

28. J. L. Tanner, D. Mousadakos, K. Giannakopoulos, E. Skotadis and D. Tsoukalas, Nanotechnology, 2012, **23**, 285501.

29. J. Lee, S. Kim, J. Lee, D. Yang, B. C. Park, S. Ryu and I. Park, Nanoscale, 2014, **6**, 11932–11939.

30. J. Park, Y. Lee, J. Hong, Y. Lee, M. Ha, Y. Jung, H. Lim, S. Y. Kim and H. Ko, ACS nano, 2014, **8**, 12020-12029.

31. J. Viventi, D. Kim, L. Vigeland, E. S. Frechette, J. A. Blanco, Y. Kim, A. E. Avrin, V. R. Tiruvadi, S. Hwang, A. C. Vanleer, D. F. Wulsin, K. Davis, C. E. Gelber, L. Palmer, J. Van der Spiegel, J. Wu, J. Xiao, Y. Huang, D. Contreras, J. A. Rogers and B. Litt, Nat Neurosci, 2011, **14**, 1599-1605.

32. J. Wang, J. Jiu, M. Nogi, T. Sugahara, S. Nagao, H. Koga, P. He and K. Suganuma, Nanoscale, 2015, **7**, 2926–2932.

33. J. Yang, J. Chen, Y. Su, Q. Jing, Z. Li, F. Yi, X. Wen, Z. Wang and Z. L. Wang, Adv. Mater., 2015, **27**, 1316–1326.

34. K. K. Sadasivuni, A. Kafy, L. Zhai, H. U. Ko, S. Mun and J. Kim, Small, 2015, **11**, 994–1002.

35. K. S. Kim, Y. Zhao, H. Jang, S. Y. Lee, J. M. Kim, K. S. Kim, J.-H. Ahn, P. Kim, J.-Y. Choi and B. H. Hong, Nature, 2009, **457**, 706–710.

36. Kenry, J. C. Yeo and C. T. Lim, Microsystems & Nanoengineering, 2016, **2**, 16043.

37. Koji Abe, Koji Suzuki and Daniel Citterio, Analytical Chemistry, 2008, **80**, 6928-6934.

38. Kyoung Il Lee, Byungjik Lim, Se Wook Oh, Seong Hyun Kim, Churl Seung Lee, Jin Woo Cho and Yongtaek Hong, MEMSYS, 2014, 963-966.

39. Kim D H, Lu N, Ma R, et al. science, 2011, **333**, 838-843.

40. L. Chiesi, P. Kejik, B. Janossy and R. S. Popovic, Sensors and Actuators A: Physical, 2000, **82**, 174-180.

41. L. K. Simone, E. Elovic, U. Kalambur and D. Kamper, in Conference proceedings: Annual International Conference of the IEEE Engineering in Medicine and Biology Society. IEEE Engineering in Medicine and Biology Society. Conference, 2004, **7**, 4791–4794.

42. L. Lin, Y. Xie, S. Wang, W. Wu, S. Niu, X. Wen and Z. L. Wang, ACS nano, 2013, **7**, 8266-8274.

43. L. Meng, S. Fan, S. Milad Mahpeykar and X. Wang, nanoscale, Royal Society of Chemistry, 2013, **9**, 1257-1262.

44. L. Meng, S. M. Mahpeykar, Q. Xiong, B. Ahvazi and X. Wang, RSC Adv., 2016, **6**, 85427–85433.

45. L. Y. Shao, A. Laronche, M. Smietana, P. Mikulic, W. J. Bock and J. Albert, Opt. Commun., 2010, **283**, 2690–2694.

46. Linzhi Tang and Nae Yoon Lee. A facile route for irreversible bonding of plastic-pdms hybrid microdevices at room temperature. Lab on a Chip, 2010, **10**, 1274-1280.

47. M. G. Broadhurst and G. T. Davis, Ferroelectrics, 1984, **60**, 3-13.

48. M. Knite, V. Teteris, A. Kiploka and J. Kaupuzs, Sensors and Actuators A: Physical, 2004, **110**, 142-149.

49. M. Park, H. Kim and J. P. Youngblood, Nanotechnology, 2008, **19**, 055705.

50. N. Hu, T. Itoi, T. Akagi, T. Kojima, J. Xue, C. Yan, S. Atobe, H. Fukunaga, W. Yuan, H. Ning and Y. Liu, Carbon, 2013, **103**, 221903.

51. N. Luo, W. Dai, C. Li, Z. Zhou, L. Lu, C. C. Y. Poon, S. C. Chen, Y. Zhang and N. Zhao, Advanced Functional Materials, 2016, **26**, 1178-1187.

52. N. Marsi, B. Majlis, A. Hamzah and F. Mohd-Yasin, Microsyst Technol, 2015, **21**, 319-330.

53. Obitayo W, Liu T. Journal of Sensors, 2012, **15**, 2012.

54. P. EAKKACHAI, K. Rabenorosoa, M. Rakotondrabe and N. Andreff, Micromachines, 2016, **7**, 1-29.

55. P. K. Panda, Journal of Materials Science, 2009, **44**, 5049-5062.

56. P. Marin-Franch and A. Peláiz-Barranco, Journal of Applied Physics, 2005, **97**, 034104.

57. Phys.org - News and Articles on Science and Technology; Available from https://phys.org/news/2015-05-inkjet-kesterite-solar-cells.html

58. Pinterest; Available from https://www.pinterest.com/pin/169518373454375529/

59. R. F. Pease and S. Y. Chou, JPROC, 2008, **96**, 248-270.

60. R. Lawes, MEMS Cost Analysis, Pan Stanford, Singapore, 2016.

61. R. Puers, Sensors and Actuators A: Physical, 1993, **37**, 93-105.

62. R. Yang, S. Xu, C. Xu, Y. Qin, Z. L. Wang and Y. Wei, Nature Nanotechnology, 2010, **5**, 366-373.

63. S. C. B. Mannsfeld, B. C. Tee, R. M. Stoltenberg, C. V. H. Chen, S. Barman, B. V. O. Muir, A. N. Sokolov, C. Reese and Z. Bao, Nature materials, 2010, **9**, 859-64.

64. S. C. Millasseau, R. P. Kelly, J. M. Ritter and P. J. Chowienczyk, Clin. Sci. (Lond)., 2002, **103**, 371–377.

65. S. Gong, D. T. H. Lai, B. Su, K. J. Si, Z. Ma, L. W. Yap, P. Guo and W. Cheng, Advanced Electronic Materials, 2015, **1**, 1400063.

66. S. Harada, K. Kanao, Y. Yamamoto, T. Arie, S. Akita and K. Takei, ACS nano, 2014, **8**, 12851-12857.

67. S. Khan, L. Lorenzelli and R. S. Dahiya, JSEN, 2015, **15**, 3164-3185.

68. S. Patel, H. Park, P. Bonato, L. Chan and M. Rodgers, Journal of NeuroEngineering and Rehabilitation, 2012, **9**, 21.

69. S. Yao and Y. Zhu, nanoscale, Royal Society of Chemistry, 2014, **6**, 2345-2352.

70. T. C. Chang, K. H. Wu, C. L. Liao, S. T. Lin and G. P. Wang, Polymer Degradation and Stability, 1998, **62**, 299-305.

71. T. Shyr, J. Shie and Y. Jhuang, Sensors (Basel, Switzerland), 2011, **11**, 1693-1705.

72. T. Yamada, Y. Hayamizu, Y. Yamamoto, Y. Yomogida, A. Izadi-Najafabadi, D. N. Futaba and K. Hata, Nature Nanotechnology, 2011, **6**, 296-301.

73. Taeksoo Ji, Soyoun Jung and V. K. Varadan, LED, 2007, **28**, 1105-1107.

74. Takao Someya, Tsuyoshi Sekitani, Shingo Iba, Yusaku Kato, Hiroshi Kawaguchi, Takayasu Sakurai and George M. Whitesides, Proceedings of the National Academy of Sciences of the United States of America, 2004, **101**, 9966-9970.

75. W. B. Dobie, P. C. G. Isaac and G. O. Gale, A-to-Z Guide to Thermodynamics, Heat and Mass Transfer, and Fluids Engineering, 2006, **18**, 117-118.

76. W. Gao, S. Emaminejad, H. Y. Y. Nyein, S. Challa, K. Chen, A. Peck, H. M. Fahad, H. Ota, H. Shiraki, D. Kiriya, D.-H. Lien, G. A. Brooks, R. W. Davis and A. Javey, Nature, 2016, **529**, 509–514.

77. W. Honda, S. Harada, T. Arie, S. Akita and K. Takei, Advanced Functional Materials, 2014, **24**, 3299-3304.

78. W. Hu, X. Niu, R. Zhao and Q. Pei, Applied Physics Letters, 2013, **102**, 38.

79. W. W. Nichols, Am. J. Hypertens., 2005, **18**, 3–10.

80. W. Yeo, Y. Kim, J. Lee, A. Ameen, L. Shi, M. Li, S. Wang, R. Ma, S. H. Jin, Z. Kang, Y. Huang and J. A. Rogers, Advanced materials (Deerfield Beach, Fla.), 2013, **25**, 2773-2778.

81. X. Jiang, Y. Sun, Z. Fan and T. Zhang, ACS nano, 2016, **10**, 7696-7704.

82. X. Xiao, L. Yuan, J. Zhong, T. Ding, Y. Liu, Z. Cai, Y. Rong, H. Han, J. Zhou and Z. L. Wang, Advanced Materials, 2011, **23**, 5440-5444.

83. Y. Jiang, S. Li, Z. M. Wang and J. Wu, Nanoscale sensors, Springer, 2014.

84. Y. Joo, J. Byun, N. Seong, J. Ha, H. Kim, S. Kim, T. Kim, H. Im, D. Kim and Y. Hong, nanoscale, Royal Society of Chemistry, 2014, **7**, 6208-6215.

85. Y. Khan, A. E. Ostfeld, C. M. Lochner, A. Pierre and A. C. Arias, Advanced Materials, 2016, **28**, 4373-4395.

86. Y. Lai, B. Ye, C. Lu, C. Chen, M. Jao, W. Su, W. Hung, T. Lin and Y. Chen, Advanced Functional Materials, 2016, **26**, 1286-1295.

87. Y. Wang, R. Yang, Z. Shi, L. Zhang, D. Shi, E. Wang and G. Zhang, ACS nano, 2011, **5**, 3645-3650.

89. Y. Zang, F. Zhang, C. Di and D. Zhu, Mater. Horiz., 2015, **2**, 140-156.

90. Yongcun Hao, Weizheng Yuan, Jianbing Xie and Honglong Chang, The Institute of Electrical and Electronics Engineers, Inc. (IEEE) Conference Proceedings, 2016, 1-3.

91. Z. Dang, M. Jiang and H. Xu, Applied Physics Letters, 2007, **90**, 042914.

92. Z. Fekete, Sensors and Actuators B: Chemical, 2015, **215**, 300-315.